UNIVERSIDADE DE LISBOA
FACULDADE DE CIÊNCIAS
DEPARTAMENTO DE FÍSICA

Adsorption of colloidal particles on mobile rafts

Diogo Estêvão Pereira Pinto

Mestrado em Física
Física da Matéria Condensada e Nano-materiais

Dissertação orientada por:
Professor Doutor Nuno Araújo
Professora Doutora Margarida Telo da Gama

2017

Acknowledgements

I would like to thank Nuno Araújo and Margarida Telo da Gama, for introducing me to the topic of physics far-from-equilibrium, for which I grew very found off, and also for their hard work, persistence and for standing by my side through this whole process. I would also like to thank Cristóvão Dias, André Nunes and Francisco Braz for their helpful input. Finally, I would like to give a special thanks to my parents and Ana Sofia for always being present. This objective was only made possible because I have a great group of people supporting me.

I would like to acknowledge the financial support from the Portuguese Foundation for Science and Technology (FCT) under Contract no. IF/00255/2013.

Abstract

Colloidal particles trapped at oil-water interfaces interact through long-range capillary forces resulting from the deformation of the interface. As a result, kinetically trapped structures are obtained and expected quasi-2D thermodynamic phases are rarely obtained. A scheme was recently proposed to avoid such strong particle-particle interactions and to obtain a fully ergodic quasi-2D colloidal dynamics. The idea is to adsorb DNA-coated colloidal particles on complementary DNA patches that are diffusing on the surface of the oil droplets. Here, we develop a theoretical model that replicates the relevant physical properties of the experimental system.

We perform an extensive numerical study of the model using a kinetic Monte Carlo algorithm. We find that the coverage, for an earlier stage of the evolution, does not depend strongly on the diffusion coefficient. However, as time evolves differences become evident. We also observe that as the system reaches jamming, the number of parameters that describe the coverage evolution can be reduced. We supplement this study with an analytical approach using a mean-field approximation. With it, we are able to reach closed form equations that describe the time evolution of the density of adsorbed particles and patches, and show that the numerical data follows the same functional dependency. We also show that our results are able to reproduce, qualitatively, what is seen in the experiments.

Finally, we use a one-dimensional continuum model to study numerically the irreversible adsorption of particles on the patches, with the focus on the possible configurations created due to the random sequential adsorption. Here, we study how the number of adsorbed particles on the patch depends on the ratio between their respective sizes. We support this study with an analytical approach, which enumerates the possible configurations of the model for certain patch sizes. We show that the analytical results are in very good agreement with the numerical ones.

KEYWORDS:
Colloidal particles, systems far from equilibrium, random sequential adsorption.

Resumo

Nesta tese é apresentado um estudo da adsorção de partículas coloidais cobertas com ADN, em gotas de óleo funcionalizadas com o ADN complementar. Este sistema visa reduzir a deformação da superfície da gota causada pela adsorção das partículas coloidais. Usando este método, é possível evitar o aparecimento de forças capilares de longo alcance entre partículas coloidais adsorvidas na interface, que leva à formação de estruturas presas pela cinética. Assim, é possível desenvolver um sistema em que a dinâmica das partículas após a adsorção é ergódica, e as estruturas termodinâmicas mais estáveis estão acessíveis pela cinética.

O sistema físico consiste em gotas de óleo submersas numa solução aquosa, estabilizadas por moléculas SDS. Na sua superfície são adsorvidas cadeias de polímeros PLL-PEG-bio, que podem difundir ao longo da superfície da gota. Depois, cadeias únicas de ADN são introduzidas aos polímeros, de modo a formar *patches* de ADN. Cobrindo as partículas coloidais com as cadeias de ADN complementares, é possível introduzir uma interação seletiva entre as partículas e a superfície da gota. Usando este método, é possível mostrar que a deformação da superfície da gota se torna desprezável. A adsorção das partículas na superfície da gota, apesar de muito forte, pode ser revertida aumentando a temperatura. Experimentalmente, observa-se que a cobertura da gota não só depende da dinâmica na sua superfície mas também da concentração de partículas coloidais em solução.

Para estudar este sistema, foi desenvolvido um modelo teórico que tenta capturar as suas propriedades físicas mais relevantes. Este consiste num substrato, modelado como uma rede, com um certo tamanho em unidades de sítios de rede, onde os *patches* difundem, com um dado coeficiente de difusão D. As partículas tentam adsorver no substrato com um fluxo F. Estas só podem adsorver em *patches* que estejam livres, e, tanto a interação partícula-partícula como a interação *patch-patch* são considerada como de volume excluído. Depois de uma partícula adsorver se ainda possuir espaço não ocupado por baixo da mesma, outro *patch* que esteja a difundir pode encontrá-la e agregar-se a ela. Usando este modelo é possível estudar a adsorção irreversível das partículas coloidais nos *patches*, e ver como a cobertura da gota depende dos parâmetros do sistema.

Uma das nossas abordagens a este problema foi numérica. Para seguir a dinâmica do sistema usámos o método de Monte Carlo cinético. Como sabemos todos os processos que podem acontecer e as respetivas taxas, é possível gerar um catálogo de processos, e assim formular um algoritmo sem rejeições. Este é bastante útil, pois possibilita a exploração de escalas de tempo mais longas de uma forma bastante eficiente quando comparado com outros método como Dinâmica Molecular. Este método faz uso de um relógio físico e tem em conta toda a sequência de eventos até chegar à configuração final (ao contrário de MC *standard*), fornecendo informações fundamentais para estudar a dinâmica.

Nós estudámos este modelo em uma e duas dimensões. Em ambas os *patches* são modelados como monómeros, enquanto que as partículas para 1D são dímeros e em 2D quadrados com largura igual a dois em unidades de sítios de rede. O nosso foco foi direcionado para a evolução temporal da

cobertura, onde observámos que a mesma aumenta monotonicamente ao longo do tempo. Também observamos que, para fluxos altos, a cobertura no *jamming* tende para o valor assimptótico de uma partícula por *patch*. Isto deve-se ao facto de que quando F aumenta os *patches* vão ter menos tempo para se agregarem entre adsorções sucessivas. Também observámos que diminui com o aumento do coeficiente de difusão, dado que este aumenta a probabilidade de *patches* se agregarem, o que diminui o número de *patches* livres em que as partículas podem adsorver.

Para tempos baixos, verifica-se que a cobertura do sistema tem uma dependência desprezável no coeficiente de difusão dos *patches*. Esta observação vem do facto de as curvas da cobertura em função do tempo, para diferentes coeficientes de difusão, quase se sobreporem à de $D = 0$. Assim, é possível definir um tempo, t^*, que mede como as curvas da cobertura para diferentes D se desviam da de $D = 0$. É possível observar que t^* decresce com D, dado que quanto maior D mais rápido os *patches* encontram outras partículas adsorvidas, produzindo um efeito na cobertura do sistema. Para além disso, t^* também decresce com n_0 (definido como a densidade inicial de *patches*), porque quanto maior n_0, menor a distância típica entre *patches*, o que promove a sua agregação. t^* também decresce com F, dado que este aumenta o número de tentativas de adsorção de partículas, levando a uma mais rápida cobertura do sistema. Estes resultados foram observados tanto para uma dimensão como para duas.

O passo seguinte foi estudar o estado de *jamming*. Aqui observámos que o número de parâmetros relevantes para o sistema quando ele chega ao *jamming* é reduzido. Enquanto que durante a dinâmica inicial tanto F como D são parâmetros relevantes, ao chegar ao *jamming* o parâmetro relevante passa a ser a razão F/D. Também observámos que a cobertura no *jamming* cresce monotonicamente com F/D, devido à competição entre as duas escalas de tempo envolventes: o tempo browniano característico da difusão dos *patches* e o tempo de chegada das partículas à interface. Sendo assim, quando F/D aumenta mais partículas vão conseguir adsorver, dado que vai ser menos provável que os *patches* consigam encontrar partículas para agregar entre adsorções sucessivas. Este resultado foi observado para uma e duas dimensões. Este resultado vem ao encontro do que foi observado experimentalmente, onde se vê que aumentar a concentração de partículas coloidais na solução (que corresponde a um aumento de F neste modelo), leva a um aumento da cobertura da gota.

Também abordámos o problema analiticamente usando uma aproximação de campo médio, de modo a estudar a evolução temporal da densidade de partículas adsorvidas (cobertura) e de *patches* livres. Tendo em conta apenas os processos de adsorção de partículas e agregação de *patches*, e desprezando as correlações espaciais, é possível chegar a duas equações exatas para o nosso problema.

Tirando o limite assimptótico ($t \to \infty$) das equações, é possível observar que o número de parâmetros necessários para descrever a densidade de partículas adsorvidas (que é igual à cobertura) é reduzido, passando de F e D, para F/D. Também estudámos o comportamento inicial das funções expandindo-as em torno de $t = 0$, onde observámos que os primeiros dois termos da expansão não dependem de D, e este parâmetro só surge no termo de terceira ordem. Por isso, enquanto o termo de terceira ordem é desprezável, a densidade de partículas adsorvidas evolui aproximadamente como observado para $D = 0$. Comparando os resultados analíticos com os da simulação usando o modelo de rede é possível observar as mesmas dependências funcionais nos parâmetros, tanto para uma dimensão como para duas.

O último estudo que esta tese foca é a descrição do sistema no contínuo. Para este estudo, propomos um modelo em que as partículas são modeladas como segmentos de um certo tamanho e o *patch* também como um segmento com de tamanho diferente. As únicas interações tidas em conta são as de volume excluído entre partículas. Para estudar este modelo numericamente, um algoritmo

foi desenvolvido que se foca na localização de intervalos abertos onde partículas podem adsorver no *patch* sem sobrepor outras. Assim é possível formular um algoritmo eficiente sem rejeições. Este estudo tem como objetivo compreender como a cobertura do *patch* depende da razão entre os tamanhos das partículas e do *patch* (AR). Observamos que para $AR > 1$, o número de partículas adsorvidas aumenta monotonicamente com o AR. No entanto para $0 < AR < 1$, dado que uma única partícula pode cobrir completamente o *patch*, a dependência em AR é diferente.

Também desenvolvemos uma abordagem analítica que se foca na enumeração de todas as possíveis configurações . Aqui apresentámos os cálculos para $0 < AR < 1$ e $1 < AR < 2$. Comparando com os obtidos numericamente observámos que ambos estão em excelente acordo.

Contents

List of Figures

Acronyms

SDS	Sodium Dodecyl Sulfate
PLL-PEG-bio	Polylysine-g-Polyethyleneglycol-biotin
RSA	Random Sequential Adsorption
kMC	kinetic Monte Carlo
BD	Brownian Dynamics
MC	Monte Carlo
RNG	Random Number Generator
AR	Aspect Ratio

Chapter 1

Introduction

With the sustained development of new technologies, experiments have been able to reach smaller and smaller scales, down to the nano-scale. This development provides the tools to synthesize new devices with enhanced physical properties and to study systematically previously observed phenomena. For example, it was possible to uncover the mechanism responsible for the change of skin color of certain reptiles, like chameleons. Today we know that the color change is related to changes in the structure of the skin (structural color) and not to the chemical composition (pigments), as initially hypothesized [1, 2]. What was observed is that they rapidly change color by actively deforming an array of small crystals, with typical sizes of the order of the wavelength of light, on the surface of their skin, which in turn changes the wavelength of the reflected/diffracted light.

The physical properties of a material depend strongly on the spatial arrangement of their individual constituents. Thus, there has been a sustained interest on developing experimental strategies to synthesize materials with a fine control over their structure. Colloidal particles are very popular for this goal [3–7], mostly because currently available techniques allow us to synthesize them in large amounts with very good control over their shape and size [8, 9]. Furthermore, they are ideal building blocks for optical materials since they have a typical size of the order of the wavelength of light. One method that can be used to control the structure is self-assembly, which designates the process through which larger structures are spontaneously formed from their smaller constituents, by taking advantage of the properties present in the constituents themselves and without the application of external perturbations. This method has received significant attention from the scientific community [10–15], since on one hand, it is less expensive than other methods to produce materials at small scales, and, on the other, it is easier to scale up and achieve massive production.

One example of a challenge in self-assembly is the formation of ordered, quasi-two-dimensional patterns of many distinct colloidal or nano particles. One promising route is to use substrates as a support for the growth of planar structures [16–20]. For that, the substrate must be smooth at the colloidal scale (micron) and the colloidal particles need to be able to bind independently and irreversibly to the surface. Another important detail is that the adsorbed particles should be mobile enough so that the most stable (thermodynamic) structures are kinetically accessible. For strong enough particle-substrate interactions, the mobility of particles after adsorption is compromised, hindering an ergodic dynamics of particles on the substrate. Under such conditions, the obtained structures are strongly dependent on the kinetics of adsorption on the substrate [3].

Methods based on the adsorption on solid substrates have been considered to synthesize materials for a wide range of applications, like quantum dots, photonic crystals, sensors, heterogeneous catalysts and microarrays [21–24]. For example, by using pre-patterned substrates it is possible

to control the dynamics of the adsorbed particles and induce local order in the first adsorbed layers [17, 21, 25, 26]. A problem with this kind of approach is that the strength of particle-substrate interaction is either very strong, and mobility after adsorption is compromised, or too weak and one cannot guarantee irreversible binding to the substrate, compromising the success of the strategy.

One alternative is the adsorption of colloidal particles on liquid-liquid interfaces, such as an oil droplet in water, forming a Pickering Emulsion [27, 28]. Using thermodynamic arguments, it is possible to show that the colloidal particles on the interface are energetically favored, as the surface energy is reduced by several k_BT [18, 27, 28]. However, as the particles will deform the interface, to guarantee a constant contact angle, long-range capillary inter-particle forces will emerge [29, 30], which promote a strong particle-particle attraction, leading to the formation of kinetically arrested structures that are significantly different from the thermodynamic ones.

To avoid strong capillary interactions and achieve an ergodic dynamics of the colloidal particles, we have proposed a method based on DNA mediated interactions [31]. By covering the surface of the oil droplet with single strands of DNA and the colloidal particles with the complementary ones, it is possible to create a selective particle/substrate interaction. A key aspect of this system is that the DNA strands are mobile and therefore the particles, after adsorbing, will be able to move without significantly deforming the interface. Using this method, the adsorption of colloidal particles to the interface is still very strong though reversible, since above a certain temperature the two DNA strands in the double helix structure unbind from each other.

Experimentally, using this strategy, it is observed that the coverage of the oil droplets is not only dependent on the dynamics on its surface but it depends also on the bulk concentration of colloidal particles in solution [31]. Given the irreversible nature of the bond formation with the substrate (for fixed temperatures), we are dealing with a system out of equilibrium and so the connection between these quantities is not trivial and should be significantly different from the classical Langmuir (reversible) dynamics. Unfortunately, it is hard to explore a large range of the parameter space in experiments due to resource (materials and time) constraints. Also, to study the dynamics it is necessary to use individual particle tracking methods which can be quite complex to implement, specially in the bulk. Thus, we developed a theoretical approach to shed light on the dynamics of this system. Combining analytic calculations with simulations, it is possible to explore systematically a wider region of the parameter space as well as to follow the dynamics, and therefore shed light on the experimental results and guide new experiments.

Numerically, we employed a kinetic Monte Carlo method to simulate the adsorption of the colloidal particles on the surface of the oil droplet. By relating the bulk concentration of colloidal particles to the rate at which they attempt adsorption on the substrate, we are able to develop a stochastic model that enables us to analyze the kinetics of adsorption. In this way, it is possible to explore how the coverage of the surface evolves in time and how it depends on the dynamical parameters of the model. The behavior of the model is discussed for one- and two-dimensional lattices. We also discuss a continuum limit focused on the adsorption of particles on a single DNA patch, with the goal of understanding the different configurations that are possible to create and how they depend on the size of the particles and of the patch.

The thesis is organized as follows: In Chapter 2, the physical system and the theoretical model is defined. Chapter 3 includes details about the simulation techniques used and some code validation examples. In Chapter 4, we report on the kinetics of adsorption on a lattice. In Chapter 5, we discuss the continuum limit of the model. In Chapter 6, some concluding remarks are drawn.

Chapter 2

The Physical System

2.1 DNA-functionalized colloidal particles and oil droplet

Many systems have been explored where DNA functionalized fluid surfaces have been used. For example, functionalizing vesicles or fluid membranes with single-stranded DNA [32, 33], or functionalizing fluid membranes enveloping hard spherical colloidal particles [34]. The motivation for using fluid substrates is to ensure that the grafted single strand DNA can diffuse on its surface without significantly deforming it, which leads to fully ergodic colloidal dynamics after adsorption. With this, it is possible to use the fluid surface as substrate for the adsorption of colloidal particles functionalized with the complementary DNA, which then self-assemble into ordered or amorphous structures depending on the experimental conditions [35–39].

Our approach (Fig. 2.1) begins with the production of oil droplets with a typical diameter of 20 to 30 μm, stabilized by sodium dodecyl sulfate (SDS), which are molecules with a hydrophilic tail and hydrophobic head group. Thus, after they adsorb on the interface of the oil droplet they form a micelle which will be used as substrate for the DNA patches. To it, a comb-like poly-electrolyte (PLL-PEG-bio) is adsorbed. As illustrated in Fig. 2.1, the positively charged poly-lysine backbone adsorbs in a flat manner onto the negatively charged SDS head-groups that are exposed to the oil-water interface. Half of the roughly 40 PEG chains per PLL backbone carry a biotin group, which are functionalized with streptavidin from solution. Finally, single strands of DNA are brought onto the oil droplets surface via the streptavidin. Thus, it is possible to create small flat patches of PLL molecules (DNA patches) that diffuse freely with their DNA on the droplets surface. When 0.57 μm large polystyrene particles with the complementary single strand DNA, are added to the solution they anchor reversibly to the surface via DNA hybridization. An important aspect of this method is that since the colloidal particles are larger than the DNA patches, after one adsorbs, the DNA patches that are diffusing can find this adsorbed particle and accumulate bellow it forming 'rafts', with complementary functionalization. After the adsorption process, the rafts formed bellow the particles are still able to diffuse with the particle attached.

There are three important experimental observations: first, the adsorption of the colloidal particles on the interface is mediated by DNA; second, this hybridization between colloidal particles and complementary DNA on the surface of the oil droplets is thermally reversible; third, the adsorbed colloidal particles diffuse on the surface of the oil droplet [31].

With this method it is also possible to show that one can control the surface coverage of oil droplets by colloidal particles, by exploiting the fact that during slow adsorption, compositional arrest takes place well before structural arrest occurs, as the diffusion of the rafts is almost negligible

within the time scale of colloid adsorption. Also, the diffusion of the rafts is, at least, one order of magnitude smaller than the one of the patches. Thus, it is possible to separate the theoretical analysis into two different time scales. A fast one, where compositional arrest occurs, corresponding to the adsorption of particles to the surface of the oil droplets, and a slow one that corresponds to the structural arrest and represents the aggregation of the colloidal particles. In this thesis, we will focus on the first one. For details about the second, please refer to [31].

Another relevant observation from the experimental data was that the coverage of the oil droplets by colloidal particles not only depended on the dynamics on its surface but also on the bulk concentration of colloidal particles in solution. The motivation for the work in this thesis comes from this experimental observation, and on the following chapters our results will be presented with the goal of studying the fast regime of the experiment, the kinetics of adsorption.

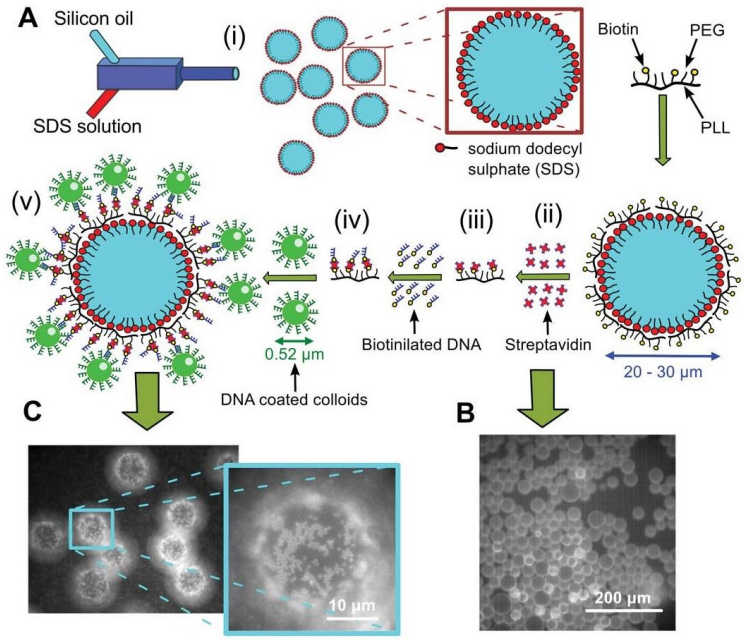

Figure 2.1: A) Representation of the various stages of the sample preparation: i) SDS stabilized droplets are prepared by mixing SDS and silicone oil in a microfluidic device.(ii) PLL-PEG-Biotin adsorbs flat on the SDS stabilized oil droplets that are negatively charged due to the sulfate head group of the SDS surfactant (iii) streptavidin linkers are then attached to the Biotin heads on the oil droplets from solution, (iv) biotinylated single strand DNA, A, is then added attaching to these streptavidin linkers. (v) Green fluorescent colloidal particles coated, with complementary A' DNA, are then allowed to bind by DNA hybridization. B) Fluorescence images of the oil droplets after attaching the streptavidin from solution, and C) a typical image showing the colloidal particles hybridized to the OD surfaces with a zoom onto the south pole of the droplet.

One possible application for this kind of methods is in the fields of medicine and biology, for drug delivery systems. Here, the objective is to encapsulate a given drug and transport it in the blood stream, without leaks. Then, when it reaches the targeted area, by applying an external perturbation, the capsule opens and the drug is released in a controlled fashion. By studying how the coverage of the system depends of the relevant parameters we can see how to create a more efficient coverage of the oil droplet and synthesize a good vessel for this type of transports. Since the adsorption of

colloidal particles is mediated by DNA, then it would also be easier to apply an external perturbation, like an increase of temperature, to release the drug in the targeted area.

2.2 The model

The objective of this work is to study the adsorption of colloidal particles on the surface of an oil droplet. After describing the experimental method used, it is important to device a model which is able to grasp all the relevant features of what it is observed experimentally while, at the same time, simple enough to be studied both numerically and analytically.

We consider a substrate which is represented as a two-dimensional square lattice with a certain lateral size L in units of lattice sites. This substrate represents the surface of the oil droplet, where the DNA patches can diffuse. We consider a two-dimensional substrate as, first, one of the interests of this work is to study the formation of quasi-two-dimensional structures, and second, the size ratio between the droplet and the DNA patches is very large and thus the effects of the curvature of the oil droplet can be considered negligible within the time scale of interest. Also, the colloidal particles are larger than the patches and after adsorption they are still able to diffuse, but since we are only interested in the initial adsorption, the dominant dynamics comes from the DNA patches which have a much higher diffusion coefficient than the adsorbed colloidal particles. Thus, we consider that, after adsorption, the diffusion coefficient of the colloidal particles is negligible.

After the oil droplet is synthesized, comb-like polymers (PLL-PEG-bio) are adsorbed on its surface to form the DNA patches. In our model, they are represented as squares with a certain length S_{patch}, in units of lattice sites. They diffuse on the lattice with a certain diffusion coefficient D, which corresponds to the rate at which they hop between neighboring sites. This rate is related to the diffusion coefficient of the DNA patches in the physical system, which depends on the temperature and viscosity of the solution, as well as the size of the patches. Thus, a change in these properties experimentally can be reflected on this model by a change of this rate. While diffusing, the patch-patch interaction is considered to be excluded volume and therefore they cannot overlap. This means that the patch-patch interaction can be, approximately, accounted for by purely geometrical restrictions. This excluded volume constraint represents an interaction which is assumed to be a short-range repulsion on a length scale shorter than the patch size. We name free patch as one which a particle has not adsorbed on yet, while after adsorption we name the combination of the patch plus the particle adsorbed on it as a patch-particle complex (or just complex).

The colloidal particles are also represented as squares with a certain size S_{part}, in units of lattice sites. They attempt adsorption on the substrate with a flux F, defined as the rate, per unit time, per unit area of deposition attempts of particles. We do not take into account the possible trajectories of the colloidal particles before adsorption since they are not relevant for this study. It is only necessary to know the rate at which they attempt to adsorb, which depends on the bulk concentration of colloidal particles in solution, since the more particles there are the more likely it is for one to adsorb, which translates into a higher flux in this model. Other properties that are also related with the flux are the temperature and pressure, and the mass of the particles. We consider that the particle-particle interaction is excluded volume and therefore they cannot overlap. Particles cannot adsorb on empty spaces of the substrate, they can only adsorb on free patches. As stated previously, after a particle adsorbs on a free patch a complex is formed and the adsorption is considered irreversible, i.e, we assume that particles do not detach or diffuse within the time scale of interest. It is important to note that, experimentally, the adsorption is reversible only by increasing the temperature of the solution

which makes the DNA strands in the double helix configuration dissociate, but in this study we are not interested in this process. Thus, the model only reflects the experimental system for temperatures below the DNA melting temperature.

Since the colloidal particles are modeled as squares, if $S_{part} > 1$, then after a colloid-patch complex is formed, the particle can still have space bellow it that is unoccupied by the patch (or multiple patches). This can happen because in our model, for an adsorption to occur, it is only necessary that the particle touches the patch in at least one site. Thus, another free patch that is diffusing can find this unoccupied space and aggregate to the complex. Depending on the size of the patch, the complex can increase its overall size after the aggregation but the number of particles remains the same (equal to one).

If $S_{patch} > 1$, after a colloid-patch complex is formed, it is possible that some area of the patch is not occupied by the particle adsorbed on it. Since the particles cannot diffuse on top of the patches after adsorption, this means that there is still space on that complex where another particle can adsorb. After more than one particle adsorbs on a complex, we consider that a cluster is formed. In summary, a complex is defined as one particle adsorbed on one or more patches, while a cluster is defined as a structure with more than one particle connected by one or more patches. As stated previously, after formation, the complexes cannot diffuse and therefore a cluster will also be considered immobile. This means that there are only two possible ways a cluster can grow, either another particle adsorbs on free space on top of a patch of the cluster, or another free patch that is diffusing aggregates to unoccupied space bellow a particle of the cluster.

In Fig. 2.2 some of the rules of the model are represented for a simple case where $S_{patch} = 1$ (monomers) and $S_{part} = 2$. From left to right are, the patch diffusion and particle adsorption, as well as two prohibited processes which are the particle overlap and particle adsorption on empty space of the substrate.

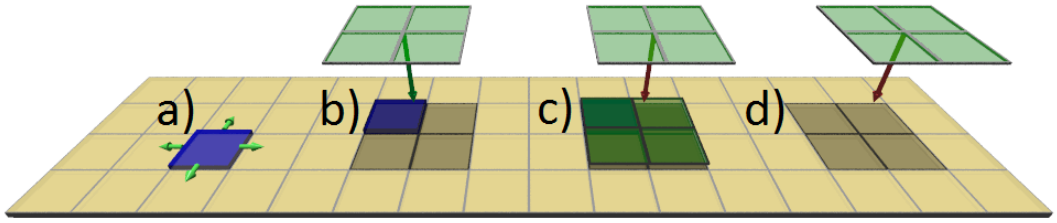

Figure 2.2: Representation of the rules of the model. In blue are the DNA patches which are modeled as monomers that are diffusing on the lattice, in green are the colloidal particles which are represented as squares with length $S_{part} = 2$ in units of lattice sites, and adsorb on top of free patches. The first two processes a) and b) are allowed and correspond to the patch diffusion and particle adsorption, c) and d) are prohibited which correspond to the overlap of particles and the adsorption on empty space of the lattice.

In this thesis, we will study this model in two and one dimensions, the only difference for one dimension is that the patches are restricted to move along a line (instead of a plane). Our study focuses on the simple case where $S_{patch} = 1$ and $S_{part} = 2$, this can be a good approximation to the experiments in the case where the size of the colloidal particles are much larger than the ones of the DNA patches so that every patch is fully covered by a particle. It is also important to note that

for this choice of parameters it is impossible to form clusters, since there can never be more than one particle per patch. We will focus mostly on the study of the time dependent dynamics as well as the jamming state, which corresponds to the state where no more particles can adsorb (no more free patches available).

This model is related to the classical Random Sequential Adsorption (RSA) model [40–52]. Here, we have the random irreversible adsorption of particles of a given size, which interact by excluded volume, similar to other RSA models. The main difference is the fact that they only adsorb on free mobile patches.

Chapter 3

Numerical implementation

Ideally, simulations should reproduce natural phenomena in the most accurate way. Unfortunately, just by estimating the computational power necessary for simulating even the simplest systems, we realize that this is impossible. For example, consider a mole of an ideal gas in a cubic box. To track the trajectories of every single particle in this system, it would be necessary to save all their positions in the memory of the computer. A mole corresponds to 10^{23} atoms, so we would need at least 10^{24} bytes. Besides, it would also be necessary to know all their velocities, so another 10^{24} bytes would be required. This amount of memory space is currently unavailable, thus, new methods are needed to access the relevant time and length scales, while still grasping the relevant physics.

After elaborating a model that is able to capture the important properties of a physical system, it is necessary to study it. One way is analytically, where one uses mathematical tools to describe the system, but for the systems that we are studying here, which are far from equilibrium, an exact analytical approach is rarely possible. So most findings are numerical, and thus numerical tools and algorithms are necessary.

To construct an efficient algorithm there needs to be a great understanding of the problem at hand. An efficient algorithm needs to lead us to results that are as accurate as possible in a reasonable amount of time. The best approach is to reduce the number of irrelevant instructions, which in turn reduces the required computational effort. For that, the most important step is to define the time and length scales where relevant processes occur, because only then it is possible to device a model and algorithm that grasps the most relevant features of the problem in an efficient manner.

This first step was already presented in chapter 2, where we gave a thorough description of the model and all the processes of relevance. With this information, we find a technique that best adapts to our problem. It is important to note that we are dealing with a model, where fluctuations play a relevant role, and so randomness needs to be taken into consideration. Thus, a statistical description of the possible outcomes is the meaningful approach to the problem in opposition to a deterministic one. The most common techniques are Brownian Dynamics and Monte Carlo methods.

Brownian Dynamics (BD) consists of calculating the individual trajectories of all the particles in the over damped regime. For this, it is necessary to know the initial conditions, and also how they interact with each other so it is possible to calculate the forces between them. Currently, these requirements are not restrictions, since even by limiting the amount of particles one can simulate at a given time, it is possible to generate enough data to improve the statistics (in a reasonable time frame). Other than that, there are also many techniques that make use of efficient algorithms [53, 54] to increase the quality of the statistics, for example, a popular approximation to use is to, instead of considering the interaction between all pairs of particles, only consider pairs of particles within

a cut-off radius. This kind of approximation considerably increases the efficiency of the algorithm without notably affecting the results. But for each case, it is necessary to evaluate which degrees of freedom are relevant and which ones can be coarse grained. First, the interactions between all the constituents of the model can be simply described as excluded volume, so the advantage that this technique has of always taking into account the particle-particle interactions is not relevant for us. Second, as stated in the previous chapter, the adsorption of the particles occurs in a much larger timescale than the particle dynamics on the surface of the droplet, therefore we consider that it is not necessary to consider the motion of particles. Finally, the worst disadvantage of this technique is the time scales that are reachable. A standard BD simulation has typical time steps of the order of $10^{-7}s$, so if we want to study events that happen in time scales of the microsecond (or larger), the computational power necessary becomes too demanding for current computers.

We decided to consider a Monte Carlo (MC) method, instead. This makes use of random sampling to compute the average of the different observables [55]. This is a more suited technique for our approach since it reduces the complexity necessary to implement BD (with MC it is not necessary to explicitly calculate the trajectories of the particles towards the substrate but solely considers an effective adsorption rate), and also, since we want to study the long time behavior, by using MC we can reach the final configuration of the system in a more reasonable time frame. But we did not use the standard MC method, we chose a more specific method named kinetic Monte Carlo (kMC). Standard MC does not take into account the physical time of the simulation nor the sequence of events leading to the final configurations. This is a problem when studying an out-of-equilibrium system, because the relevant physical properties depend on the kinetics leading to the final configuration. Thus, we use kMC, since it has a physical clock and the sequence of events corresponds to a possible sequence of events in the physical system [56–58]. The obtained configurations are not necessarily the ones with the lower free energy (the ones obtained in equilibrium through MC), but the ones obtained kinetically.

With kMC it is possible to formulate a rejection free algorithm that improves the overall performance of the simulations, when compared to standard MC. For this, we only need to know the rates for all the processes and, as described in the previous chapter, this is set by the model. Another relevant advantage of it is that it lets us define a physical time, which is a very important property when studying the kinetics of adsorption and when comparing to experimental results. To define the physical time it is necessary to relate the rates used in the algorithm with the ones measured experimentally.

3.1 Kinetic Monte Carlo

The algorithm, for the kMC, was coined N-fold way since processes are classified into N different classes, based on their transition probabilities, or rates in our particular case. It was first proposed by Bortz, Kalos and Lebowitz, in 1975, for the simulation of Ising spins [59]. At that time, the problem they faced was that, for low temperatures, the amount of rejections the MC algorithms needed to simulate the system was very large, which means that there would be many irrelevant steps before the relevant physical properties could manifest. Thus, they introduced a rejection free algorithm to address this numerical challenge.

Since we are dealing with a stochastic model, the dynamics of the components will be random between different simulations, even for the same set of parameters. Thus, if we analyze the data from a single evolution, the results can display distinct features that are not characteristic of a typical

evolution and are only a product of statistical fluctuations. To avoid these features, when measuring the results, the quantities of interest are taken by averaging over many samples.

The algorithm starts by generating a two-dimensional square lattice with size L in units of lattice sites (as explained in chapter 2). Then this lattice needs to be occupied by a certain density of patches. Thus, it is necessary to generate a random configuration of free patches distributed in an uncorrelated fashion. We use the random number generator (RNG) Marsenne Twister from the Boost C++ Libraries, to generate pseudo-random numbers. We chose this RNG because it has a very long period ($2^{19937}-1$), which means that it is necessary to make a high number of iterations for the RNG to start repeating itself, and also, it has passed numerous tests for statistical randomness [60].

The first step of the algorithm is to define which processes can happen, in our case (using the model in Chapter 2) we have patch diffusion and particle adsorption, but since the lattice the patches need to be distributed, another process is introduced, which is the patch adsorption. To make this simpler, the simulation is divided into two parts, a first one where the patches are adsorbing on the lattice and at the same time diffusing (after adsorption) and a second one where we have the necessary density of patches already adsorbed, which we define as n_0, and so the particles are allowed to adsorb while the patches stop, and are only allowed to diffuse. The diffusion coefficient rate is always set to a given value, since the patches are allowed to diffuse in both the first and second part of the simulation. The reason why we let the patches diffuse while they are adsorbing is so that their initial distribution is uniform and does not depend on the adsorption sequence.

3.1.1 Initial conditions

As stated, the simulation is divided into two parts, the first corresponds to the adsorption of the patches on the substrate, and represents the initial conditions. To implement this, we use the kMC algorithm.

First, a catalog of all the possible processes that can occur is created. For that it is necessary to sweep all lattice sites to identify what processes can happen in them. Since the lattice starts without patches, the only process that can happen is patch adsorption, therefore the catalog corresponding to that process will have all lattice sites in it, while the catalogs for the other processes are empty. Thus, a patch is adsorbed, and for that a random number is generated between 0 and the size of the catalog that corresponds to the process of patch adsorption, and the patch is generated in the site corresponding to that, randomly selected, entry in the catalog.

After a process is performed the catalogs need to be updated since the system configuration has changed. After a patch adsorbs, a new one cannot adsorb in that site, so the entry corresponding to it in the patch adsorption catalog is removed. As stated previously, in this first part of the simulations, we want the patches to diffuse, therefore we add an entry to the patch diffusion catalog corresponding to this site. To increase the efficiency of the algorithm, we start to build the catalog of particle adsorption as well, during this first part, so an entry is also added to it, since this patch is free. It is important to note that, although the particle adsorption catalog starts being developed in this part, it will only be taken into account in the second part of the simulation, since the particle adsorption rate, in this first part, is set to zero. It is also necessary to update other sites that are affected by this patch, for example, if $S_{patch}=1$ and $S_{part}=2$, then after the patch adsorbs the first and second neighbors of this site also need to be added to the particle adsorption catalog since one can adsorb there and still touch the patch.

Now there are two possible processes that can occur, patch adsorption and diffusion. To choose

which process to perform next, the cumulative rate is calculated:

$$C_i = \sum_{j=1}^{i} n_j W_j \ , \tag{3.1}$$

where n_j is the number of components that can perform a certain process j, and W_j the rate for that process. C_N, where N is the total number of processes, is the total rate. Since currently we only have two processes, $N = 2$,

$$C_N = \sum_{j=1}^{N} n_j W_j = n_{PA} W_{PA} + n_{PD} W_{PD} \ , \tag{3.2}$$

where PA corresponds to the process of patch adsorption and PD to the one of patch diffusion.

To select the next process, a random number, r, uniformly distributed in the interval $]0, 1]$, is generated and the process is chosen by finding the i which satisfies the inequality:

$$C_{i-1} < r C_N < C_i \ , \tag{3.3}$$

then the process is performed by selecting the respective catalog and generating a random number between zero and the total number of entries in it, the entry selected will correspond to a specific site on the lattice that will perform the process. Finally, the different catalogs are updated. This way, no rejection occurs, which leads to an increased efficiency of the algorithm.

This algorithm is iterated until the density of patches reaches n_0. After this happens, the initial conditions are generated. The time and the rate of patch adsorption are set to zero, and the rate of particle adsorption is increased.

3.1.2 Algorithm for the kinetics of adsorption

When the initial conditions of the model are generated, which corresponds to a density of n_0 patches adsorbed, the second part of the simulation begins. This corresponds to the particle adsorption on the free patches which are diffusing on the substrate. As mentioned, to increase the efficiency of the algorithm, we construct the catalog for patch adsorption while generating the initial conditions, but we did not take it into account when evaluating the possible processes in that part. Now it is necessary to do so.

Since both catalogs (patch diffusion and particle adsorption) are already constructed, it is possible to perform a process. For that, the cumulative rate is calculated again, as presented in Eq. 3.1, but now the processes possible will be different when calculating the total rate:

$$C_N = \sum_{j=1}^{N} n_j W_j = n_{PtA} W_{PtA} + n_{PD} W_{PD} \ , \tag{3.4}$$

where PtA corresponds to particle adsorption and PD is patch diffusion. A new random number is generated and the process is chosen by using Eq. 3.3, but now with the values from Eq. 3.4. Then the process is performed by selecting the respective catalog and generating a random number between zero and the total number of entries in it, the entry selected will correspond to a specific site on the lattice that will perform the process. After the catalogs are updated, the algorithm is iterated.

3.1.3 Time incrementation

Since we are interested in studying the time dependent dynamics, time needs to be incremented in the appropriate way.

Given a certain time increment Δt, $P(\Delta t)$ is defined as the probability of no process occurring in the interval Δt after a previous one has occurred, and C_N as the total rate of events, as defined previously using Eq. 3.1. Thus, the probability of a process to occur in the interval dt is $C_N dt$. The probability of a process to occur in the interval $[\Delta t, \Delta t + dt]$ is proportional to the probability of no process during Δt and the probability of a process occurring in the interval dt. Therefore, the probability of no process in $\Delta t + dt$ is given by [61]:

$$P(\Delta t + dt) = P(\Delta t) - P(\Delta t) C_N dt \ . \tag{3.5}$$

Solving Eq. 3.5,

$$P(\Delta t) = \exp(-C_N \Delta t) \ . \tag{3.6}$$

From Eq. 3.6, one gets:

$$\Delta t = -C_N^{-1} ln(r') \ . \tag{3.7}$$

where r' is a random number, uniformly distributed, in the interval $]0, 1]$.

3.1.4 Boundary conditions

Since we are interested in properties that happen in the bulk, it is necessary to guarantee that boundary effects are negligible, to reduce finite-size effects. Experimentally, the number of particles is large enough, so that many times, it is a good approximation to treat the system as if it was in the thermodynamic limit. However, as discussed previously, due to computational constraints, it is not possible to numerically replicate such scale of events, and we have to limit the size of our simulated system. A good approach is to use periodic boundary conditions. This means that each side of the substrate, in our case, is mapped into the opposite one. Thus, if a particle diffuses through one of the sides it will re-enter the system in the opposite side. By doing this, we are effectively considering an infinite system, where the substrate is replicated periodically. If one wants to measure the distance between sites it is necessary to take the boundary conditions into account and make the proper mapping.

It is important to stress that, although the use of periodic boundary conditions helps in reducing the finite-size effects, it might not make them negligible. Thus, it is still necessary to take these effects into consideration when measuring the relevant properties. For that, we need to make sure we are not using a system size that is too small, to the point the effects are noticeable. Thus, it is important to study the properties of interest for different system sizes. By observing when the measurements collapse to the same values, we can conclude what size we can consider so that the finite-size effects are negligible.

The algorithm explained here focused more on the use of a two-dimensional substrate, but it is also possible to adapt it to the one-dimensional case. The differences come mostly from the reduction of the possible directions, from four to two.

3.2 Code validation

After formulating an algorithm and writing the code, it is necessary to test it to check for possible problems in the implementation. In this section, results taken with the algorithm described previously are compared to known analytical and numerical results. First, we study a one-dimensional case with only the adsorption of dimers on a lattice. Then, we compare a two-dimensional implementation to the adsorption of monomers with diffusion on a lattice, using the algorithm described in the previous section, to analytical results.

3.2.1 Dimer adsorption on a one-dimension lattice

A very well known exact result in RSA is the random sequential adsorption of dimers [62, 63]. The interesting property of this system is that a vacant region that is smaller than the particle size (in this case dimers) can never be filled, which means that the substrate can reach a jammed state that cannot accommodate additional adsorption events, where the substrate is not completely covered. So it is interesting to study how the system approaches the jamming state.

The model is simple, there is a flux of particles (dimers) to the substrate, attempting to adsorb irreversibly. These adsorption attempts occur at random on the substrate, and dimers cannot overlap with each other. After each successful adsorption attempt, the coverage of the system increases, where coverage is defined as the density of occupied sites. From here, it is possible to conclude that the jamming state coverage is between $2/3$ and 1. The first corresponds to the case where there is always an empty site on the left and right of an adsorbed dimer, and the second, to the case where there are no empty sites in the lattice and, therefore, all are filled. A first result was derived by Flory [64] using a combinatorial approach, where he derived that an initially empty substrate saturates at a jamming coverage: $\rho_{jam} = 1 - \exp(-2)$. It is also possible, using an empty interval method to reach an exact analytical solution for the time dependence of the coverage, ρ [62, 63]:

$$\rho(t) = 1 - \exp\{-2[1 - \exp(-t)]\} \ . \tag{3.8}$$

In Fig. 3.1 is plotted the coverage as a function of time. In circles are the simulation results using the algorithm described in the previous section, where the only possible process is the adsorption of dimers on the substrate, and in dashed lines are the theoretical results, in green is the value for the coverage of the jammed state derived by Flory, while in blue is the exact solution in Eq. 3.8.

The results were taken for a substrate of size $L = 10^7$, in units of lattice sites. From Fig. 3.1, it is possible to conclude that our simulation results are in perfect agreement with the analytical ones. Using our simulation results, we reached a value of the jamming coverage equal to $0.864666 \pm 8 \times 10^{-6}$, which is in very good agreement with the analytical one, $\rho_{jam} = 1 - \exp(-2) \approx 0.864665$.

3.2.2 Adsorption of monomers with diffusion on a two-dimension lattice

As the dimension increases the problem becomes increasingly difficult. While there are exact analytical results for RSA in one-dimension, there are practically no exact solutions for two and three dimensions. This is mostly due to the complexity of the problem, since it is necessary to take into account all possible configurations of connected clusters of any size and then solve the coupled equations for the evolution of the probabilities that each cluster configuration is empty. Thus, most results are either achieved using simulations, or approximations like mean-field.

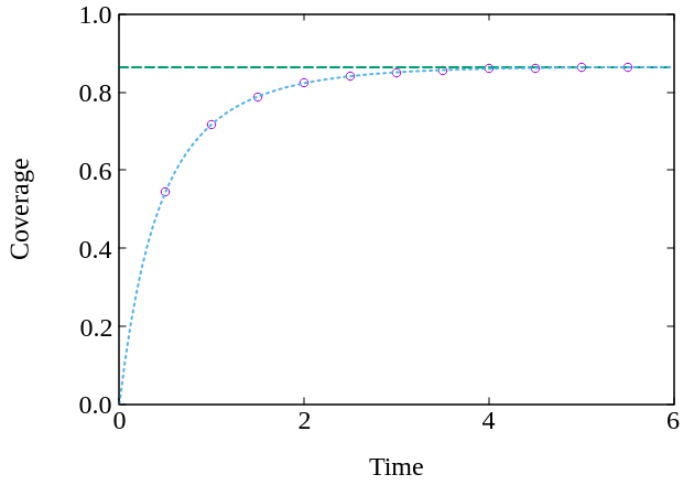

Figure 3.1: Coverage as a function of time, for dimer adsorption in a one-dimensional lattice. In circles are the simulation results, and in dashed lines are the theoretical results, in green is the value for the coverage of the jammed state derived by Flory, while in blue is the exact solution in Eq. 3.8.

To test our two-dimensional implementation using an exact analytical solution, it is necessary to consider simple systems. In this case, we simulate the adsorption of monomers on a two-dimensional lattice. The model is pretty straightforward, monomers attempt to adsorb on a two-dimensional lattice with a certain flux, and after adsorbing, they are allowed to diffuse to their nearest neighbors if they are empty. The adsorption is considered irreversible and the monomers cannot overlap.

This next step of the code validation is meant to test our implementation with more than one possible process. Although the particles can adsorb and then diffuse, since we are dealing with monomers, the diffusion coefficient should not be a relevant parameter. So the coverage needs to evolve as it would be expected for monomer adsorption only, which means that the density of occupied sites increases with time at a rate proportional to the density of vacancies:

$$\frac{d\rho}{dt} = 1 - \rho \ , \tag{3.9}$$

solving this equation we get:

$$\rho(t) = 1 - \exp(-t) \ . \tag{3.10}$$

In Fig. 3.2, it is plotted a comparison between this solution (Eq. 3.10) and the simulation results, for a two-dimensional substrate with length $L = 1000$, in units of lattice sites. It is possible to observe that the diffusion coefficient does not play a role in the results and therefore our simulation results are in perfect agreement with the analytical ones.

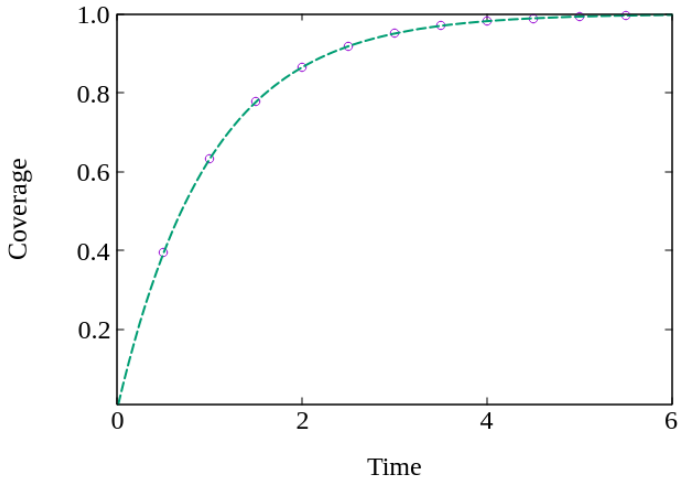

Figure 3.2: Coverage as a function of time, for monomer adsorption in a two-dimensional lattice. In circles are the simulation results, and in a dashed line is the theoretical result derived for monomer adsorption given by Eq. 3.10.

Chapter 4

Adsorption kinetics on a lattice

Our main objective is to study the kinetics of adsorption of colloidal particles on mobile patches, that diffuse on the surface of an oil droplet. For this, a model has been presented that tries to capture the most relevant physical features (see Chapter 2). We also already presented the method and algorithm we will be using to simulate it (see chapter 3). In this chapter, the results are discussed.

First, we discuss a one-dimensional case of the model presented in Chapter 2, where the particles are represented as dimers, $S_{part} = 2$, and patches as monomers, $S_{patch} = 1$. One thing to note in this case is that since the patches are monomers only one particle can adsorb on them. This means that for this set of parameters no clusters are formed. This corresponds to the limit where the colloidal particles are much larger than the patches, to the point where there can only be one particle per patch adsorbed. We will focus on the time dependent dynamics of the coverage and the jamming state. We will study also how they vary with the relevant parameters of the model, which are the patch diffusion coefficient and the flux of particles towards the substrate.

In this chapter, we will also consider the two-dimensional case. What this means is that the patches have one more degree of freedom, and the particles instead of being modeled as dimers, are squares.

We also discuss a mean-field approach to the model, to describe the time evolution of the density of free patches and adsorbed particles using rate equations. With it, we can reach closed form equations for this time dependence, which are in very good agreement with the numerical results.

4.1 Kinetics on a one-dimensional lattice

In this section, we consider the adsorption of dimers ($S_{part} = 2$) on monomers ($S_{patch} = 1$). In Fig. 4.1 there is a scheme summarizing some rules of the model in one-dimension. The model described in Chapter 2 is the same as the one used here, the major difference comes from the fact that the translational degrees of freedom are reduced.

In this case, there are only two possible configurations of complexes: one particle and one patch; or one particle and two patches. Therefore, it is not possible to form clusters, since on each patch there can only be one particle adsorbed. If we define the coverage, θ, as the density of complexes formed (number of adsorbed particles per lattice site), then, the maximum coverage is equal to the initial density of free patches. If the flux F is large enough, the diffusion of the patches is negligible, and the system is sufficiently diluted, then:

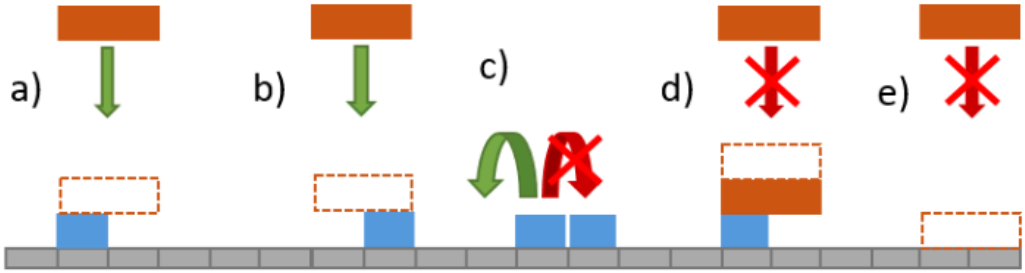

Figure 4.1: Representation of the rules of the model for one-dimension. In blue are the patches which are represented as segments of length $S_{patch} = 1$, in units of lattice sites and can diffuse on the lattice, with a certain diffusion coefficient. In orange are the particles which are represented as segments of length $S_{part} = 2$ in units of lattice sites, and adsorb on top of free patches. a) and b) represent the allowed adsorption processes for this particular pair of S_{patch} and S_{part}, then c) is a representation of the rules of diffusion for patches, d) and e) are the prohibited processes for particle adsorption.

$$\lim_{F\to\infty} \theta_j \to n_0 \ , \tag{4.1}$$

where θ_j is the jamming coverage, defined as the asymptotic coverage when there can be no more adsorption events (all free patches are occupied), and n_0 is the initial density of patches. We are also able to deduce another limit, where each particle has two patches. In this case, $\theta_j \to n_0/2$, which corresponds to a case where the time the patches have between adsorptions is so large that they are always able to aggregate to a particle-patch complex ($D >> F$).

Unless otherwise stated, all results are obtain for a substrate size $L = 10^7$, and averages over 10^4 samples.

4.1.1 Time dependent dynamics

The results are presented in Fig. 4.2, where a plot of the coverage as a function of time for a given F and D is shown. From Fig. 4.2 a), it is possible to see that the jamming coverage increases with F. As F increases the patches will have less time to diffuse during successive adsorptions, and therefore it will be more likely that a particle adsorbs on a free patch than the patch aggregating to an already adsorbed particle. As expected, when F increases the coverage will tend to the maximum value given by 4.1. In Fig. 4.2 b) it is observed that the jamming coverage monotonically decreases with D. In this case, the patches will have more time between adsorptions and therefore their probability of aggregating to a complex is higher which in turn will decrease the jamming coverage.

From Fig, 4.2 b), we can see that the curves in the initial dynamics show the same behavior and then after a certain time they diverge from each other. If we lower the initial density of patches this effect is even less noticeable, as seen in Fig. 4.3 a), for $n_0 = 0.03$. It is also possible to observe that as the diffusion coefficient increases the faster the curves deviate from each other (Fig. 4.3 b).

We argue that the patches, for low times, do not have enough time between adsorptions to aggregate to complexes and therefore the effect the diffusion of the patches has on the coverage is negligible. This is confirmed when we compare the simulation curves for $D > 0$ with one for $D = 0$. It is possible to observe two different regimes, the first where the diffusion coefficient of the patches does not seem to impact on the coverage (all curves almost overlap with the one with $D = 0$), and the second where there are significant differences. The first regime corresponds to a

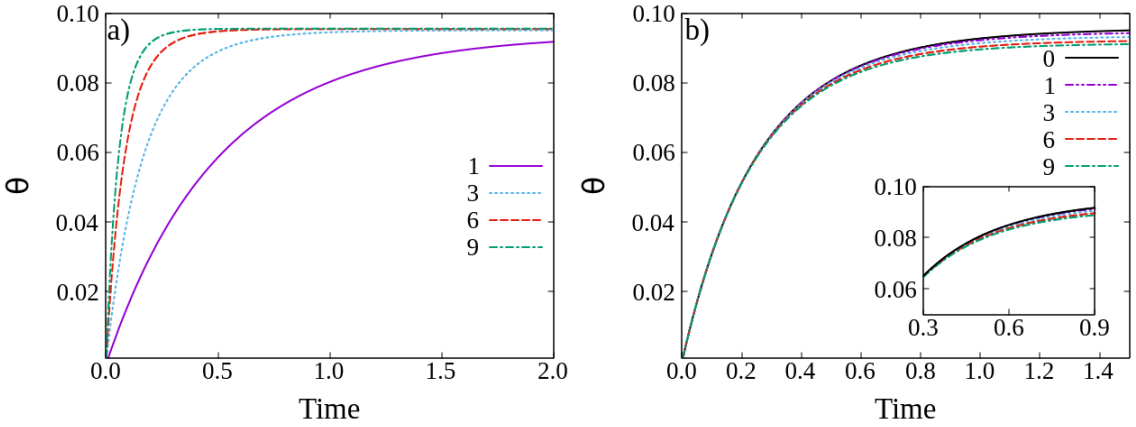

Figure 4.2: Time-dependence of the coverage for a) $D = 1$ and $F = 1, 3, 6, 9$, b) $F = 2$ and $D = 0, 1, 3, 6, 9$. The initial patch density is $n_0 = 0.1$. It is possible to observe on a) that, as F increases the jamming coverage tends to the maximum value given in Eq. 4.1 and on b) that when D is increased the jamming coverage decreases. From b) we can also see that for the initial dynamics the curves almost overlap when F is constant which means that in this regime the system behaves as $D \approx 0$.

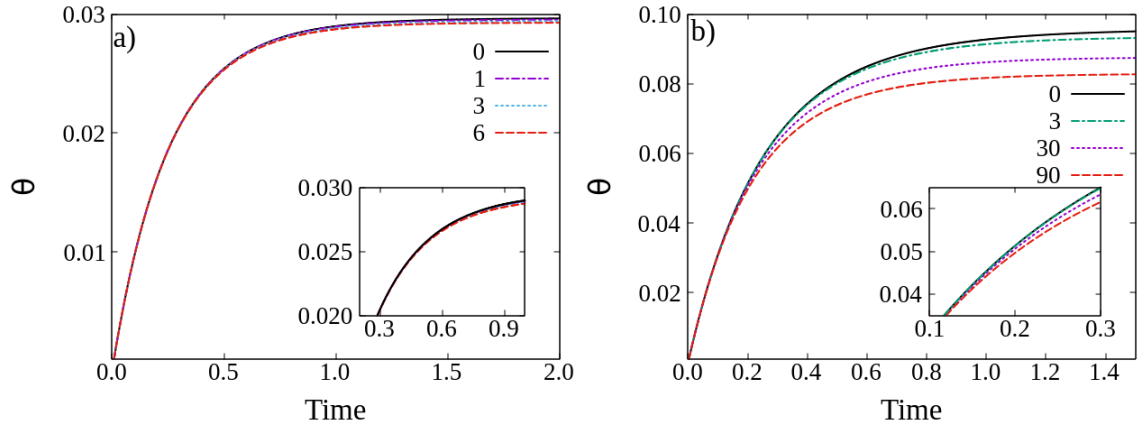

Figure 4.3: Time-dependence of the coverage for $F = 2$ and $D = 0, 1, 3, 6$, with $n_0 = 0.03$, in a), and $F = 2$ and $D = 0, 3, 30, 90$, with $n_0 = 0.1$, in b). By comparison to Fig. 4.2, we can see that as n_0 decreases the curves will stay longer in the first regime where the system behaves as $D \approx 0$. As D increases it is possible to observe that the curves diverge sooner from the $D = 0$ one.

system where $D \approx 0$, while in the second the diffusion of the patches starts to have a larger impact on the coverage evolution. This also explains why for smaller n_0 the curves deviate less from $D = 0$, because as n_0 decreases the typical distance between patches, and between complexes and patches, will increase, which means that they need more time to find complexes, and so the first regime lasts for a longer period of time.

We define a t^* as an instant of time where the coverage for a certain diffusion coefficient D differs from the one for $D = 0$ by more than ε.

$$|\theta_D(t^*) - \theta_0(t^*)| = \varepsilon \ . \tag{4.2}$$

Here, we considered $\varepsilon = 0.01$. θ_D is the coverage for a given diffusion coefficient D and θ_0 is the coverage for $D = 0$. From Fig. 4.4 one can observe that as D or n_0 increases, t^* decreases, which was already concluded from previous results. Another conclusion that we can take from Fig.

4.4 is that t^* decreases when F increases, since the higher the value of F the more particles will be able to adsorb and therefore it will be more likely for a patch to aggregate to a complex, since there are more available. Below, in section 4.3 we will provide a theoretical study to explain this behavior.

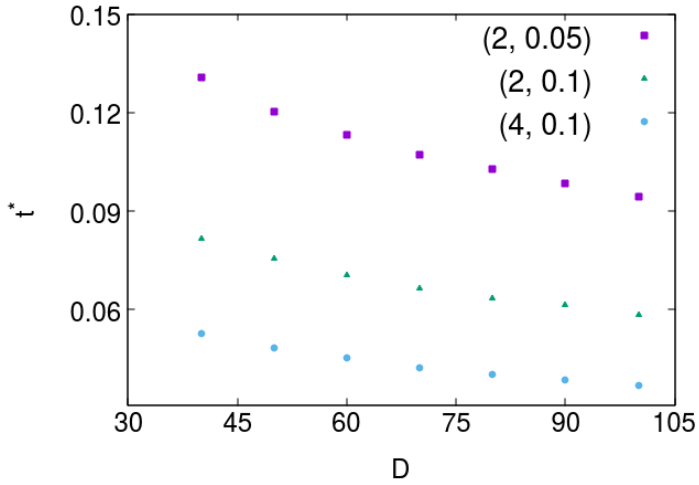

Figure 4.4: t^* as a function of D, for different sets of parameters $(F, n_0) = (2, 0.05); (2, 0.1); (4, 0.1)$. It is possible to observe that when (F, D and n_0) increase, t^* decreases.

4.1.2 Jamming state

Fig. 4.5 shows the coverage evolution for different values of F and D. It is clear that, while the kinetics depend on both values, the jamming coverage only depends on the ratio F/D, as for the same ratio the curves overlap asymptotically.

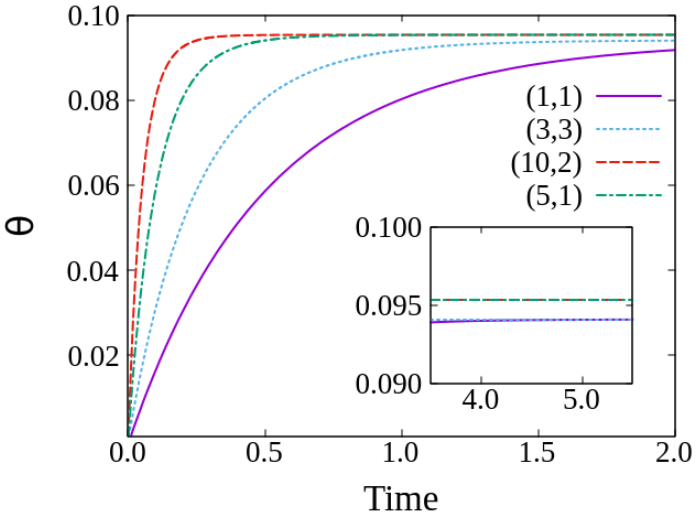

Figure 4.5: Coverage as a function of time for different F and D. It is possible to observe in the insets that when F and D change but the ratio F/D is kept the same, the curves collapse when they reach jamming.

From Fig. 4.6 a), it is possible to observe that θ_j (jamming coverage) increases monotonically with F, but decreases with D (Fig. 4.6 b). Also as F increases the system tends to the limit of one

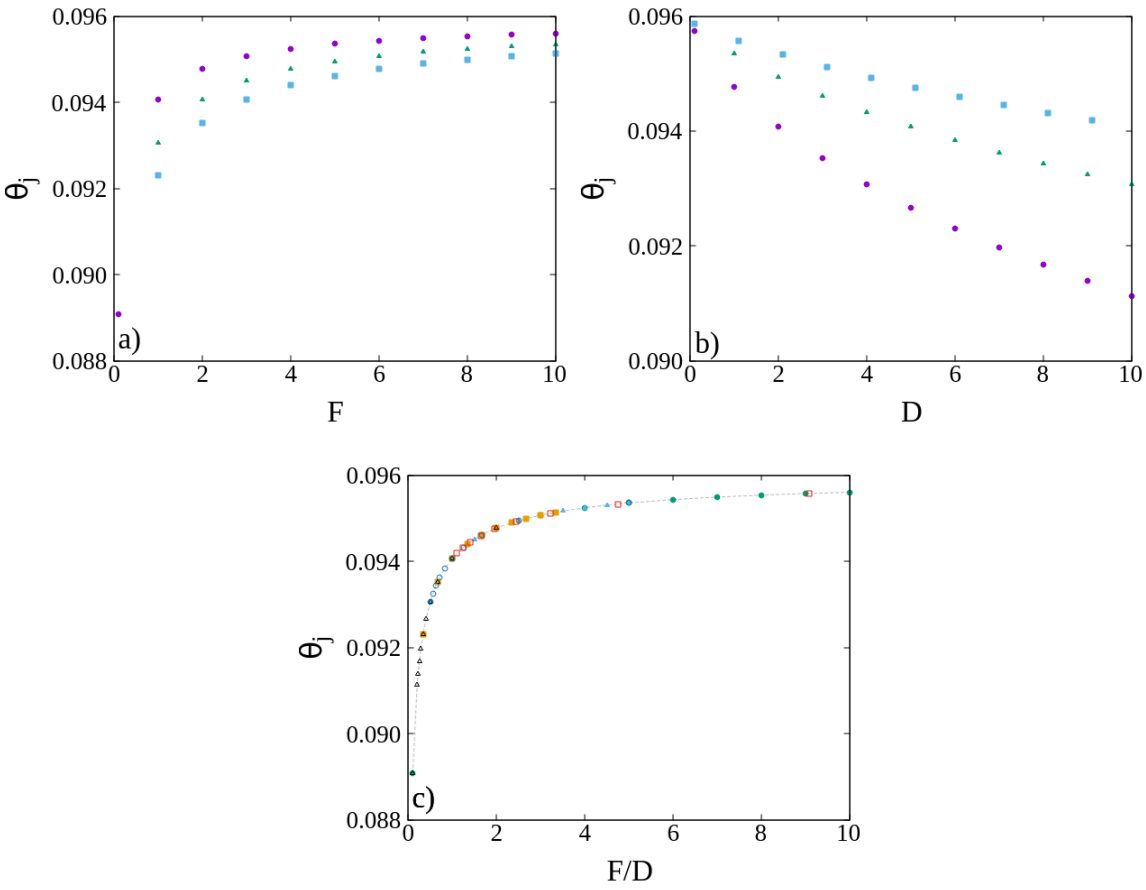

Figure 4.6: Jamming coverage as a function of a) F for $D = 1, 2, 3$, b) D for $F = 2, 5, 10$, both represented as circles, triangles and squares respectively, and c) the ratio F/D. As expected from the previous results, the jamming coverage decreases with D but increases with F. Other than that by using the parameter F/D instead, it is possible to observe a data collapse.

particle per patch, as expected.

Using the results from Figs. 4.6 a) and b), but now plotting θ_j as a function of the ratio F/D, we get a data collapse (Fig. 4.6 c). Thus, we are able to confirm, for a wider range of parameters, the result in Figure 4.5, that θ_j will only depend on the ratio F/D, and not on the pair F and D.

It is possible to observe that the jamming coverage increases monotonically with F/D. This happens because when F/D is small, the patches will have enough time to find complexes and aggregate to them between successive adsorptions, reducing the number of free patches available while not increasing the coverage. On the other hand, when F/D is larger, the patches have less time to diffuse and so more particles will be able to adsorb, which will lead to a more efficient (jamming) coverage. This effect is even more pronounced for higher initial patch densities where the typical distance between patches, or between patches and adsorbed particles, is shorter, favoring the binding of free patches to previously adsorbed particles.

In Fig. 4.7 the jamming coverage as a function of F/D is shown, for $n_0 = 0.1, 0.01$. It is possible to observe that as n_0 decreases, the jamming coverage increases. This is due to the fact that, when n_0 increases the typical distance between patches, and between patches and adsorbed particles, decreases, which promotes their aggregation. Thus, decreasing n_0 leads to a more efficient coverage.

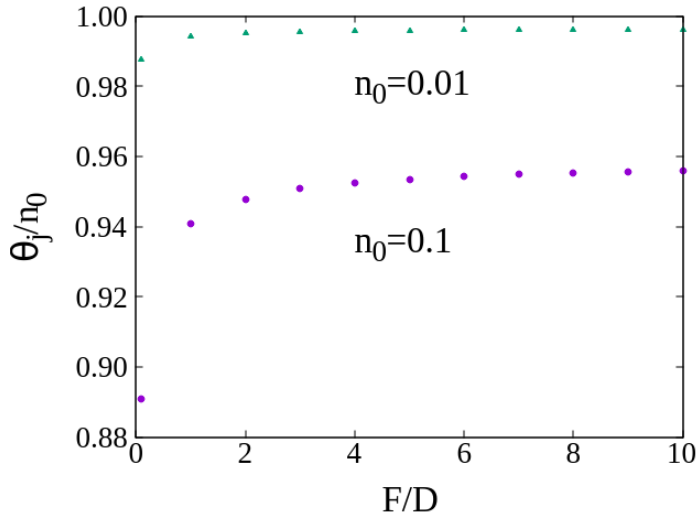

Figure 4.7: Jamming Coverage as a function of F/D for $n_0 = 0.1, 0.01$. It is possible to observe that as n_0 decreases the jamming coverage increases.

4.1.3 Finite-size study

To be able to simulate these systems in a reasonable time frame it is necessary to take into account some approximations and limit their size. Then, one of the problems that can arise is the effect of the finite size of the system in the results. These are unwanted effects, since in the real systems they are typically not relevant (they are usually near the thermodynamic limit). Thus, it is necessary to see if the results presented here can be a byproduct of the finite size of the system.

To verify if there are any finite-size effects in our results we consider three different system sizes, $L = \{10^5, 10^6, 10^7\}$. The results are presented in Fig . 4.8. It is possible to conclude from this analysis, that there are no relevant finite-size effects in the results. Thus, we can focus our study on only one system size (the largest one).

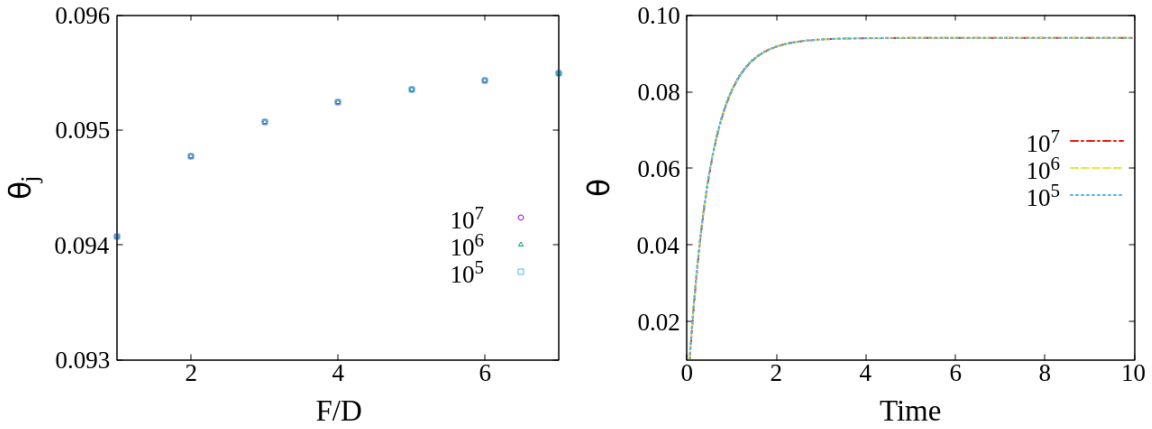

Figure 4.8: Jamming coverage as a function of the ratio F/D (a), and coverage as a function of time (b), for different systems sizes, $L = \{10^5, 10^6, 10^7\}$. It is possible to observe that all curves collapse and therefore there are no relevant finite-size effects that we need to take into account.

4.2 Kinetics on a two-dimensional lattice

The next step of this study is to increase the spatial dimension. The most notable difference for the one-dimensional case, is the increase in translational degrees of freedom, since now patches can move in two directions, but the rest of the implementation is similar.

The results were analyzed using a substrate of linear length $L = 2000$ in units of lattice sites, and averaged over 10^4 samples. In this case, the particles are modeled as squares with length $S_{part} = 2$ in units of lattice sites, while the patches are modeled as monomers, $S_{patch} = 1$. The rules of the model are the ones discussed in Chapter 2. As for the one-dimensional case, it is not possible to form clusters. In Fig. 4.9 are presented two snapshots of the simulations for two different n_0, for easier visualization the patches are represented as lattice nodes. Here, it is possible to observe some of the configurations of the system.

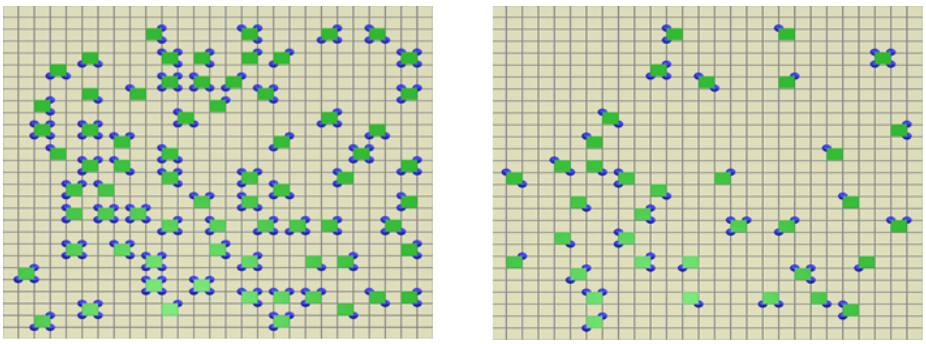

Figure 4.9: Snapshots of the simulations for two different initial patch densities, $n_0 = 0.3, 0.1$, for the two-dimensional model, with $L = 25$

From the initial conditions, it is possible to draw some conclusions about the asymptotic behaviors. First, just as in one-dimension, the maximum coverage possible is equal to the initial patch density $\theta_{max} = n_0$ (where θ is the coverage of the system, which corresponds to the density of adsorbed particles). This represents the case where the patches do not have enough time to find previously adsorbed particles. Thus, the rate of adsorption is much larger than the one for diffusion, $F >> D$. It also represents a case where the typical distance between patches, and between patches and complexes, is very large so that the particles only adsorb on single patches, which happens for low n_0. The other asymptotic value is when $\theta_{min} = n_0/4$, which corresponds to the case when for each adsorbed particle there are four different patches, and can happen for $D >> F$ or high n_0.

4.2.1 Time dependent dynamics

In Fig. 4.10, are presented the results for the coverage as a function of time, for different pairs of F and D. It can be observed that, as F increases, the jamming coverage will also increase. As explained before, patches will have less time to aggregate to complexes between adsorptions, which will lead to a more efficient coverage (Fig. 4.10 a). From Fig. 4.10 b), as D increases, the jamming coverage will decrease, since more patches will be able to aggregate to complexes. It is also possible to see that for low times the curves almost overlap, just like for 1D.

Comparing the results in Fig. 4.10 to the ones in Fig. 4.2, it is possible to conclude that the results are very similar, both showing the same qualitative results: jamming coverage increases with F and decreases with D, and for earlier times there is an overlap for different diffusion coefficients D but constant F. The most notable differences are only quantitatively, since the jamming coverage

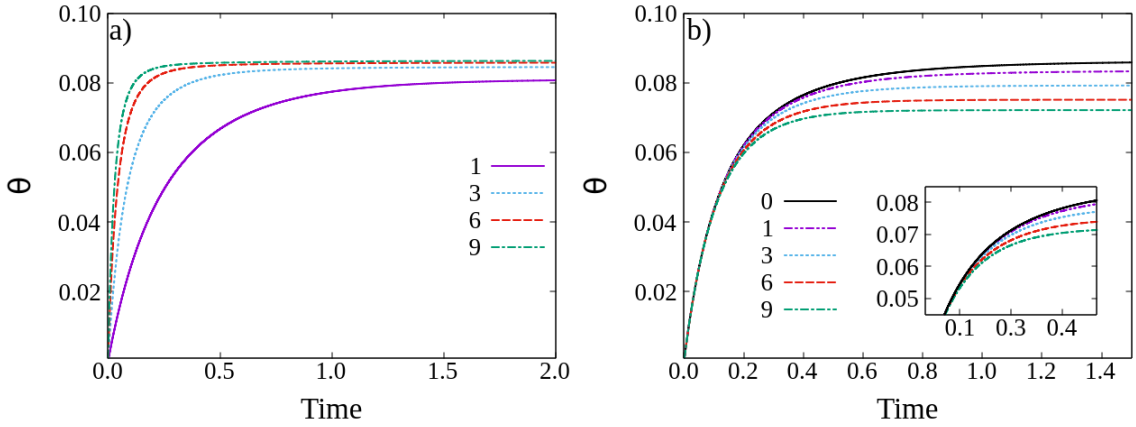

Figure 4.10: Time-dependence of the coverage for a) $D = 1$ and $F = 1, 3, 6, 9$, b) $F = 2$ and $D = 0, 1, 3, 6, 9$, for the two-dimensional system.The initial patch density is $n_0 = 0.1$. It is possible to observe on a) that, as F increases the jamming coverage tends to the maximum value, $\theta_j = n_0$, and on b) that when D is increased the jamming coverage decreases. From b) we can also see that for the initial dynamics the curves almost overlap when F is constant which means that in this regime the system behaves as $D \approx 0$.

obtained in one-dimension, for the same sets of parameters, is higher than in two. Other key aspect, is the fact that now patches can diffuse in four directions, while in one-dimension it is likely that a free patch gets confined into a region between two complexes. In two-dimensions more particles are needed to confine the patch to such a region and thus it is less probable to occur.

The curves show the collapse for low times, which was also seen in one-dimension. Thus, the same argument is applied here, the time evolution of the system can be divided into two different regimes, one where $D \approx 0$, and another where the diffusion coefficient has an effect on the coverage evolution. Here, the characteristic time t^* is also introduced as in Eq. 4.2. In Fig. 4.11 is represented t^* as a function of D, for different n_0 and F, and it is possible to conclude that t^* decreases when D, F or n_0 increases, just as seen in one-dimension.

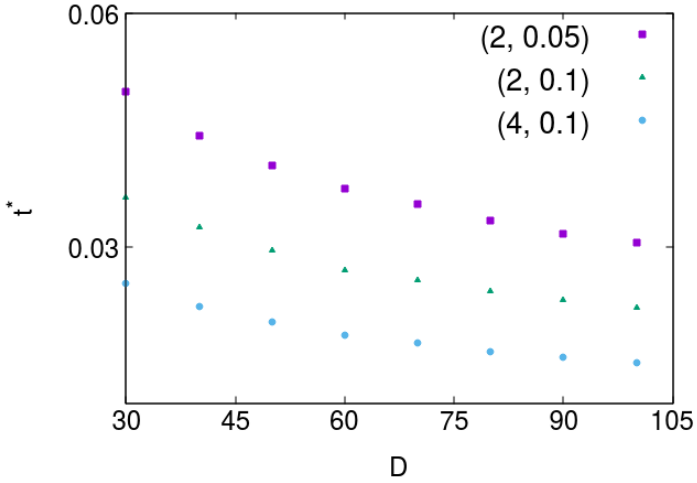

Figure 4.11: t^* as a function of D, for different sets of parameters $(F, n_0) = (2, 0.05); (2, 0.1); (4, 0.1)$, with the two-dimensional model. It is possible to observe that when the variables (F, D and n_0) increase, t^* decreases.

4.2.2 Jamming state

It can be seen, in Fig. 4.12, that the coverage depends on both F and D, but as time increases and the coverage saturates, the curves with the same ratio of F/D overlap asymptotically. From Fig. 4.13, it is possible to conclude that the jamming coverage will not depend on the pair F and D, but on the ratio F/D, thus, $\theta_j = \theta(F/D)$. For the initial dynamics, this is not observed since, for different D, but same F/D, the curves are different. Therefore the necessary number of parameters is reduced when the system reaches jamming.

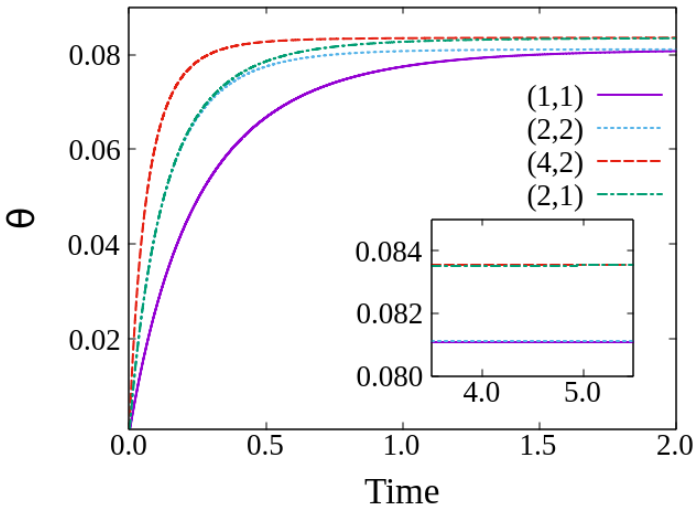

Figure 4.12: Coverage as a function of time for different F and D, with the two-dimensional lattice model. It is possible to observe in the insets that when F and D change but the ratio F/D is kept the same, the curves collapse when they reach jamming.

It is observed that as the ratio F/D increases the coverage also increases. This is due to the fact that there are two different time scales involved: one is the inter-arrival time, which sets the typical time between two consecutive attempts of particle binding per lattice site and it corresponds to the inverse of the flux, and the other is the Brownian time, that corresponds to the average time necessary for a patch to diffuse in a region corresponding to its area and it is the inverse of the diffusion time.

When F/D is small, the patches will have enough time to find unoccupied particle space and aggregate to them between successive adsorptions, reducing the number of free patches available while not increasing the coverage. On the other hand, when F/D is larger, the patches have less time to diffuse and so more particles will be able to adsorb, which will lead to a more efficient (jamming) coverage. This effect is even more pronounced for higher initial patch densities where the typical distance between patches, or between patches and adsorbed particles, is shorter, favoring the binding of free patches to previously adsorbed particles. As F/D increases the coverage tends to the asymptotic value $\theta_{max} = n_0$ and, as expected, when the density is lowered the coverage gets closer to it.

Comparing Figs. 4.12 and 4.13 to Figs. 4.5 and 4.6 c), it is possible to conclude that, just as in the time dependent dynamics, the qualitative results are the same, and these are: the jamming coverage only depends on the ratio F/D, and it is a monotonically increasing function of it. The most notable differences from one- to two-dimensions are the quantitative results. In two-dimensions the jamming coverage reached by the system is lower, for the same sets of parameters, this was also seen and

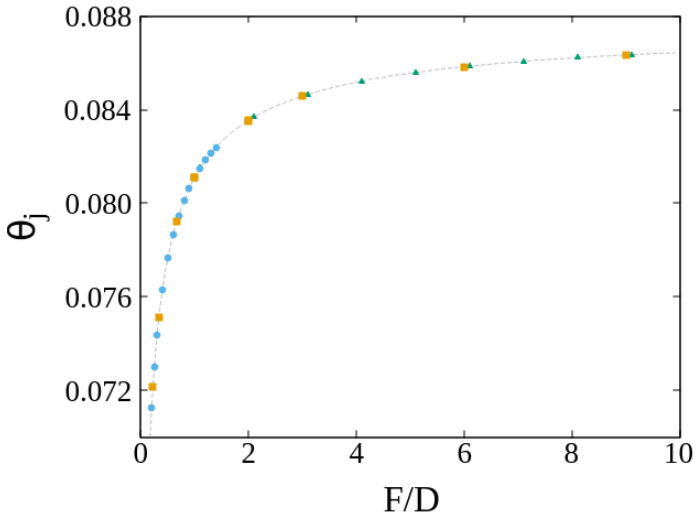

Figure 4.13: Jamming coverage as a function of the ratio F/D, for different sets of parameters F and D, for the two-dimensional lattice. As expected from the previous results, the jamming coverage decreases with D but increases with F. Other than that by using the parameter F/D instead, it is possible to observe a data collapse.

discussed in the previous section.

From Fig. 4.14, it is possible to observe that as n_0 decreases, the jamming coverage increases. This was also seen in one-dimension in Fig 4.7. It is due to the fact that, as n_0 decreases the typical distance between patches, and patches and adsorbed particles, increases, which in turn reduces the probability of patch aggregation, leading to a more efficient coverage of the system.

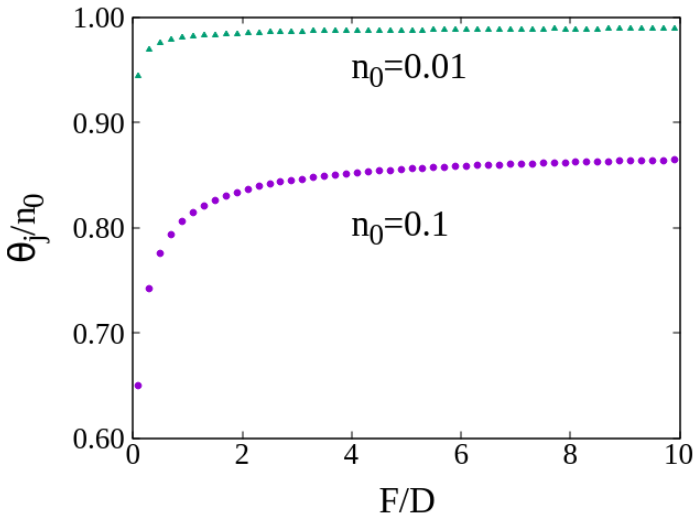

Figure 4.14: Jamming Coverage as a function of F/D for $n_0 = 0.1, 0.01$. It is possible to observe that as n_0 decreases the jamming coverage increases.

4.2.3 Finite-size study

As discussed previously, in order to simulate these physical systems it is necessary to consider some approximations and restrict the size of our systems. Unfortunately, for some models, the size

of the system can have an effect on the results, which needs to be taken into account.

To verify if there are relevant finite-size effects, we considered four different system sizes, $L = \{250, 500, 1000, 2000\}$. The results are plotted in Fig. 4.15. This shows that there are no notable size effects. Thus, we can focus our study on only one system size.

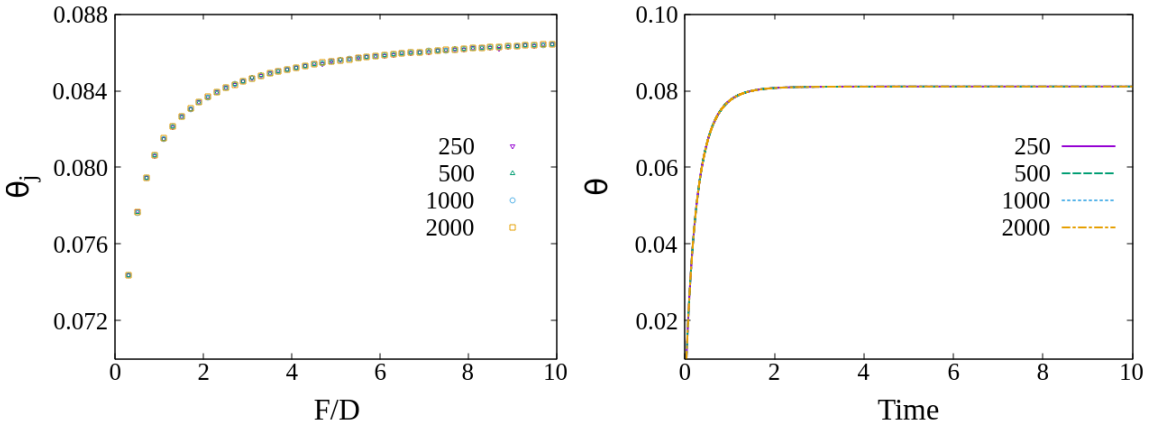

Figure 4.15: Jamming coverage as a function of the ratio F/D (a), and coverage as a function of time (b), for different systems sizes, $L = \{250, 500, 1000, 2000\}$. It is possible to observe that all curves collapse and therefore there are no relevant finite-size effects that we need to take into account.

4.3 Mean-Field approach

Let us now consider a mean-field approach to the model, based on rate equations. Accordingly, we consider that space is homogeneous and therefore the space correlations are negligible. We study the time evolution of the density of free patches (ρ_r) and of adsorbed particles (ρ_p). The latter is equal to the coverage, defined in Chapter 4 .

Initially, there is a given number of patches n_0 and no particles adsorbed. Therefore the initial conditions are:

$$\rho_r(t=0) = n_0 \,, \tag{4.3}$$

$$\rho_p(t=0) = 0 \,. \tag{4.4}$$

Then the particles will adsorb and create complexes. This means that the density of free patches only decreases in time. It decreases when a particle adsorbs on top of a patch and also when a patch aggregates to a complex. The number of particles adsorbed will only increase in time as long as there are free patches available. This translates into two rate equations:

$$\begin{cases} \frac{d\rho_r(t)}{dt} = -\overline{F}\rho_r - \overline{D}\rho_p\rho_r \\ \\ \frac{d\rho_p(t)}{dt} = \overline{F}\rho_r \end{cases} , \tag{4.5}$$

where $\overline{F}$ and $\overline{D}$ are monotonic increasing functions of the flux F and the diffusion coefficient D, respectively. These equations can be decoupled, obtaining:

$$\begin{cases} \ddot{\rho_r} + \overline{DF}\rho_r^2 - \frac{\dot{\rho_r}^2}{\rho_r} = 0 \\ \\ \ddot{\rho_p} + (\overline{D}\rho_p + \overline{F})\dot{\rho_p} = 0 \end{cases} . \tag{4.6}$$

To solve these equations it is necessary to introduce two new variables $v_i(\rho_i) = d\rho_i/dt$, where $i = r, p$. This reduces the two second order Eqs. 4.6, to first order ones. Thus, it is possible to reach an exact analytic solutions for the time dependence of the densities,

$$\rho_r(t) = \frac{\overline{F} + 2\overline{D}n_0}{\overline{D} + \overline{D}\cosh\left[\sqrt{\overline{F}(\overline{F} + 2\overline{D}n_0)}t + 2\,\mathrm{arctanh}\left(\sqrt{\frac{\overline{F}}{\overline{F}+2\overline{D}n_0}}\right)\right]} , \tag{4.7}$$

and,

$$\rho_p(t) = \frac{\sqrt{2\overline{FD}n_0 + \overline{F}^2}\tanh\left\{\frac{1}{2}\left[2\,\mathrm{arctanh}\left(\frac{\sqrt{\overline{F}}}{\sqrt{\overline{F}+2\overline{D}n_0}}\right) + \sqrt{\overline{F}}\sqrt{2\overline{D}n_0 + \overline{F}}t\right]\right\} - \overline{F}}{\overline{D}} . \tag{4.8}$$

A more detailed derivation of these equations is presented in Appendix A.

4.3.1 Initial regime and asymptotic behavior

While discussing the numerical results, we observed that the system displayed interesting properties in its initial and asymptotic limits. Thus, the next step is to see if we can reproduce these observations using this analytical approach.

The asymptotic behavior of these functions can be analyzed by taking $t \to \infty$ in Eqs. 4.8 and 4.7. Knowing the following limits:

$$\lim_{t\to\infty} \tanh(t) = 1 , \tag{4.9}$$

$$\lim_{t\to\infty} \cosh(t) = \infty , \tag{4.10}$$

and making the respective substitutions,

$$\rho_p(\infty) = \sqrt{\overline{F}/\overline{D}}\sqrt{2n_0 + \overline{F}/\overline{D}} - \overline{F}/\overline{D} , \tag{4.11}$$

$$\rho_r(\infty) = 0 . \tag{4.12}$$

From Eq. 4.11 it is possible to see that the asymptotic behavior of ρ_p will only depend on $\overline{F}/\overline{D}$, leading to the conclusion that the jamming coverage, that in this analytical model corresponds to the asymptotic limit ($t \to \infty$), will solely depend on the ratio $\overline{F}/\overline{D}$ (and n_0). Note that, it is not possible to reduce the number of parameters in both Eq. 4.8 and 4.7, since there will always be a $\overline{D}$ term inside the hyperbolic tangent and hyperbolic cosine, respectively. Thus, both $\overline{F}$ and $\overline{D}$ are relevant parameters for the dynamics. This is precisely what we observe in the simulations on a lattice (in one- and two-dimensions). The mean-field calculation still grasps this dependence on F/D.

Another result discussed before is the apparent overlap of the curves for the earlier stage of adsorption, as observed in Fig. 4.2 b). This is also observed analytically, represented in Fig. 4.8.

To understand this behavior, we make a Taylor expansion when $t = 0$:

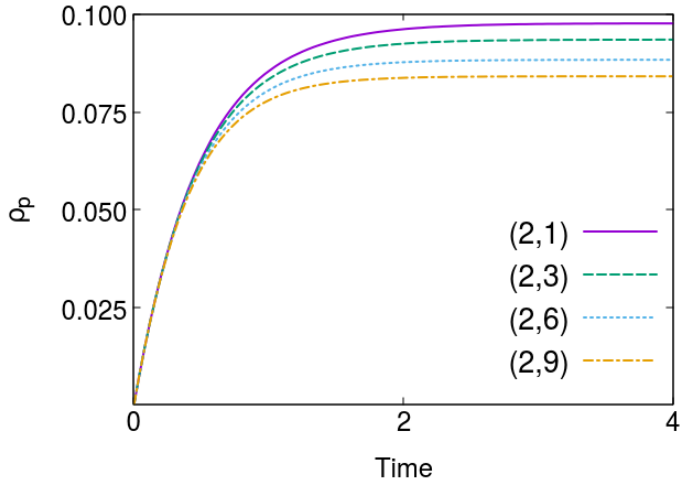

Figure 4.16: Plot of Eq 4.8 for different sets of parameters ($\overline{F}$,$\overline{D}$). It is possible to observe that for small times the curves overlap.

$$\rho_p(t \to 0) \approx t\overline{F}n_0 - \frac{t^2}{2}\overline{F}^2 n_0 + \frac{t^3}{6}(\overline{DF}^2 n_0^2 - \overline{F}^3 n_0) + O(t^4)\ . \tag{4.13}$$

It is possible to observe from Eq. 4.13 that the diffusion coefficient parameter $\overline{D}$ only appears in the third term of the expansion. Thus, for very low times, while this term is negligible, the density of particles adsorbed is unaffected by the diffusion of the patches, and the curves collapse. But when it becomes relevant, the curves diverge since they have different diffusion coefficients.

From Eq. 4.13, it is also possible to conclude that the terms that do not depend on $\overline{D}$, correspond to a Taylor expansion of an exponential increase around $t = 0$. This is something to be expected, since if $D \approx 0$, then the solution for the Eq. 4.5 is an exponential function, similar to the one presented during the code validation for monomer adsorption on an empty lattice [62].

4.3.2 Comparison between the analytical and numerical results

From the previous discussion of the analytical results, it is possible to conclude that this approach is able to capture the two main findings based on the numerical data. Let us attempt a more quantitative comparison between the two.

We start by comparing the initial behavior of the system. In the simulation we defined a time, t^*, given by Eq. 4.2. By substituting Eq. 4.13, into Eq. 4.2, it is possible to derive:

$$t^* = \left(\frac{6\epsilon}{\overline{DF}^2 n_0^2}\right)^{1/3} \tag{4.14}$$

In Fig. 4.17 there is a plot comparing this analytical result to the numerical data. It is possible to observe that, the functional dependence on the model parameters predicted by the analytical calculation are in good agreement with the numerical data for one dimension. For two-dimensions, it is possible to conclude that, while the data does not overlap for different sets of parameters, it still follows the dependency derived analytically, in Eq. 4.14.

The next step is to see if the functional dependence of the equations is preserved when comparing to the numerical data. For that, Eq. 4.8 is fitted to the numerical data. As stated previously, $\overline{F}$ and $\overline{D}$

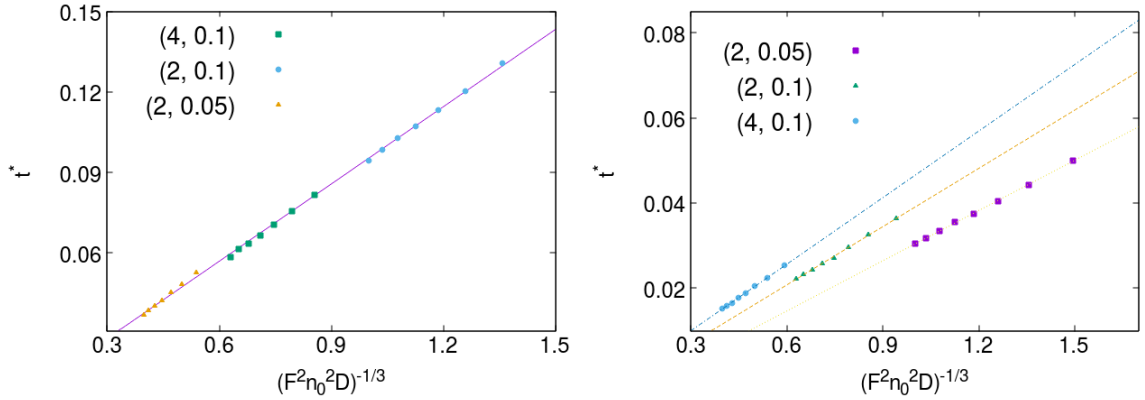

Figure 4.17: t^*, as defined in Eq. 4.2, as a function of $(F^2 n_0^2 D)^{-1/3}$, for different set of parameters $(F, n_0) = (4, 0.1); (2, 0.1); (2, 0.05)$. Comparison between the analytical and the numerical results for the one- and two-dimensional cases (left and right respectively).

are not the same as F and D, they are functions that depend on them. This is due to the fact that we are using a mean-field approximation.

In Fig. 4.18 is presented a comparison between the one- and two-dimensional numerical data and the analytical equations fitted to them. It is possible to see that the analytical solution 4.8 fits better to the one-dimensional results than the two. But still, both are in good agreement and therefore we can conclude that the functional dependence is preserved.

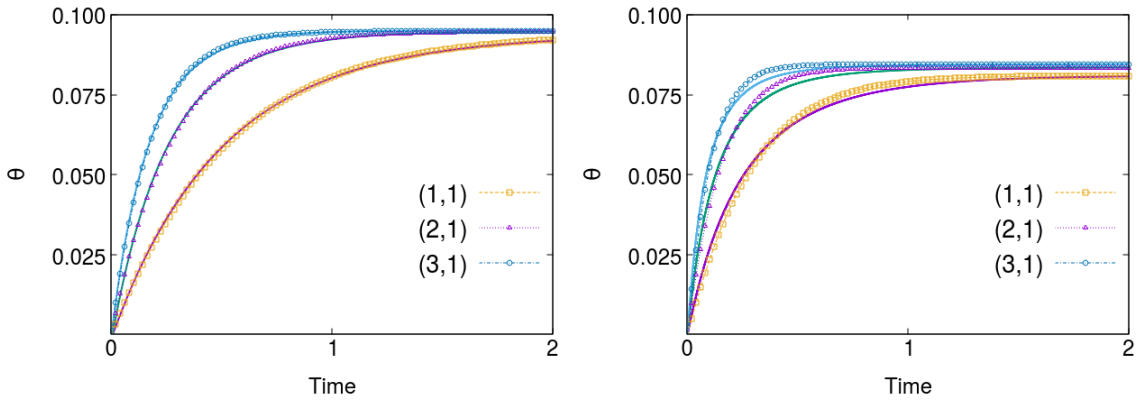

Figure 4.18: Coverage as a function of time, for different sets of parameters, $(F, D) = (1, 1); (2, 1); (3, 1)$ and $n_0 = 0.1$. Comparison between the analytical result and the numerical data for the one- and two-dimensional cases (left and right respectively).

Finally, let us analyze the asymptotic limit. As seen previously, analytically it is possible to derive that the jamming coverage does not depend on $\overline{F}$ and $\overline{D}$ independently, but on the ratio $\overline{F}/\overline{D}$, which is also observed numerically. To compare to the simulation results, a Taylor expansion of the square root, in Eq. 4.11, for $\overline{F} >> \overline{D}$ is made,

$$\begin{aligned}\rho_p(\infty) =& \overline{F}/\overline{D}\sqrt{2n_0\overline{D}/\overline{F}+1} - \overline{F}/\overline{D} \\ &\approx -\overline{F}/\overline{D} + \overline{F}/\overline{D}\left(1 + \frac{2n_0}{2\overline{F}/\overline{D}} - \frac{4n_0^2}{8(\overline{F}/\overline{D})^2} + ...\right) \\ &= n_0 - \frac{n_0^2}{2\overline{F}/\overline{D}} \ .\end{aligned} \tag{4.15}$$

A comparison between Eq. 4.15 and the simulation results for one- and two-dimensions is presented in Fig. 4.19. It is possible to conclude that the results for the lattice models, both in one- and two-dimensions, have the same functional dependence as derived in Eq. 4.15.

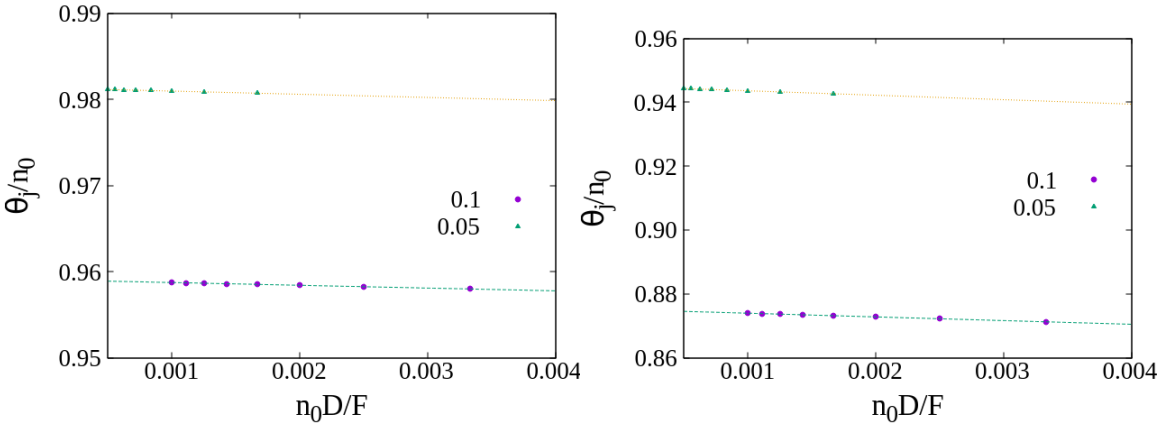

Figure 4.19: Jamming coverage as a function of the ratio F/D. Comparison between the analytical result and the numerical data for the one- and two-dimensional models (left and right respectively). It is possible to conclude that the functional dependence derived in Eq. 4.15 is preserved in the lattice model.

Chapter 5

Continuum Limit

So far, we have focused on a discrete version of the model. This enabled the use of a specific method (kMC) that not only allowed to implement an efficient algorithm, but also generate results that shed light on the experimental observations. Here, we attempt a continuum description of the system.

Until now all the relevant properties of the system depended on the kinetics and time evolution, but as the concentration of patches on the surface of the droplet is reduced, or the bulk concentration of colloidal particles in solution is increased (and therefore the rate at which they attempt adsorption increases), the kinetics of relaxation become less and less relevant since most patches will not have enough time between adsorption to aggregate, and most of the obtained structures are formed due to the kinetics of adsorption. In this case, it is pertinent to study what are the possible configurations of particles and patches, in the continuum limit.

Since we only want to enumerate the possible configurations, time is no longer relevant. We also consider a very diluted system, such that two patches do not interact with each other. Thus, we can make this study by considering only one patch with a certain size where particles can adsorb. We focus on a one-dimensional case, where particles are modeled as segments with a certain size and adsorb on a patch that is modeled as a line segment of a different size.

5.1 Adsorption on a line

In one-dimension this problem is very similar to the popular *car parking problem*, where segments of unit length adsorb irreversibly on an infinite line. Rényi obtained a jamming coverage of $\rho_{jam} = 0.747597$ [65]. It is even possible to derive an analytical expression for the time dependence of the coverage by using the empty intervals method in the continuum:

$$\rho(t) = \int_0^t \exp\left[-2 \int_0^v du \frac{1-\exp(-u)}{u} \right] dv \ . \tag{5.1}$$

This equation cannot be solved exactly but it is still possible to numerically evaluate the integrals to reach the result calculated by Rényi, as well as, to calculate the asymptotic behavior of it and see that the coverage approaches jamming as a power law.

The main difference of our problem to this one, is that we take into account the actual finite size of the substrate (in this case the patch) and see how the different configurations depend on the ratio patch size/particle size.

First, we consider the irreversible adsorption of particles with a certain size l on a continuum substrate (which represents the patch) with size r. Without lost of generality, we consider $l = 1$, i.e., we rescale all lengths in units of the particle size. The only constraint to the system is that the particles cannot overlap (excluded volume interaction). For the particles to adsorb it is only necessary that they touch the patch, so for example, if the patch starts at $x = 1$, and extends up to $x = r + 1$, in the x axis, a particle can adsorb if its leftmost point falls within the interval $0 > x > r + 1$ (since if it falls on $x = 0$, it will still extend up to $x = 1$ and touch the patch). In Fig. 5.1 is a scheme of the rules of the model.

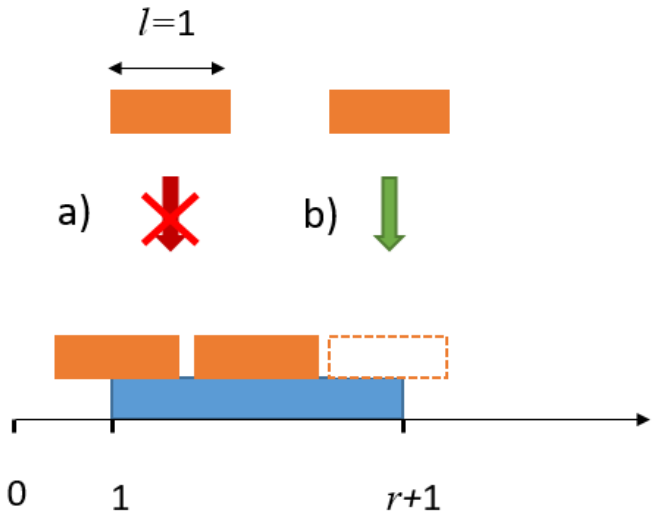

Figure 5.1: Representation of the rules of the continuum model for one-dimension. In blue is the patch which is represented as a segment of length r, and in orange are the particles which are represented as segments of length $l = 1$ and adsorb on top of the patch. a) represents a prohibited process, which is the overlap of particles, while b) represents an allowed process, which is the adsorption of a particle on top of unoccupied space of the patch

The interesting property of the one-dimensional problem is that it is possible to reach exact analytical solutions by formulating an approach that takes into account all possible configurations. Unfortunately, as r increases, this approach becomes more and more complex, therefore we only solve it for the cases where $0 < r < 1$ and $1 < r < 2$. We also present a numerical approach to the problem.

The objective of this study is to see how the average number of particles adsorbed on the patch depends on the size ratio, $AR = r/l$. Since $l = 1$, this is reduced to $AR = r$.

5.1.1 Algorithm

An efficient algorithm is constructed based on the property of the model where after particles adsorb they create empty gaps on the patch where others can adsorb. Thus, we define a gap as a segment of a certain length where a particle can adsorb on the patch without overlapping others. With this, it is only necessary to keep track of the gaps on the patch and then randomly generate a particle to adsorb on it.

First, we decided to take the reference point of every segment to be the left side. Accordingly, if a segment is put in the position $x = x_{ref}$, it will occupy the space between $x = x_{ref}$ and $x = x_{ref} + 1$ (this reference point does not necessarily need to be the left side, but it is the one we chose). Thus, every time the position where a segment falls is referred, its always referencing to this point. In order

to implement this algorithm, a substrate of length $x = r+1$ is used, where the patch spans the length between $x = 1$ and $x = r + 1$. We define substrate as the full length where particles can adsorb. We make this convention for particles can still adsorb to the left of the patch. For example, if the patch starts in $x = 1$ and a particle falls in the point $x = 0$ (reference point), its endpoint will be $x = 1$, and it will still reach the patch and adsorb (assuming it is not overlapping others).

The algorithm starts with one single gap, that ranges from $x = 0$ to $x = r + 1$, and therefore means that a particle can adsorb in any point of that gap. Then a random number between $x = 0$ and $x = r + 1$ is generated and it corresponds to the reference point of the particle that will adsorb, x_{ref}. After the adsorption, part of the gap is filled, so it is necessary to find if any other gaps were created. For that, the distance between the particle and the boundaries of the gap it adsorbed on are evaluated. First, the distance between x_{ref} (the reference point of the particle) and $x = 0$ (point where the gap starts) is evaluated: if it is larger than one, a new gap is created between $x = 0$ and $x = x_{ref} - 1$. It is important to note that when evaluating distances to the left side, the gap can only be created if this distance is larger than one. This is because our reference point is the leftmost point of the particle, so it will span a length of one from that reference point, thus if the distance of the gap is smaller than one it will overlap the already adsorbed particle.

Then the other side is also evaluated. For that the distance between $x = x_{ref} + 1$ to $x = r + 1$ (endpoint of the gap) is calculated and if it is bigger than zero then another gap is created where a particle can adsorb. Since in this case we are evaluating the distance to the right of the endpoint of the adsorbed particle, the new gap does not need to be bigger than one since another particle can adsorb anywhere after $x = x_{ref} + 1$ without overlapping any previously adsorbed particle (it can adsorb as long as it is inside the patch). If both conditions are satisfied then the old gap is discarded, and two new gaps are formed.

Since the two new gaps are on opposite sides of the adsorbed particle, successive particle adsorptions on either side will not have an effect on the opposite one. The algorithm is then iterated by adsorbing another particle on either the created gaps. The difference now comes from the fact that one particle is already adsorbed, so for example if we take the right side, where the gap spans the length between $x = x_{ref} + 1$ to $x = r + 1$, then a random number is generated in this interval and a particle is generated in the point $x = x_{2;ref}$. Since the particle will divide the gap, the old one will be discarded, and new gaps will be created. For that the distances between the reference point of the new adsorbed particle and the beginning of the old gap are evaluated, as well as, the distance between the end of the adsorbed particle and the end of the old gap. If they satisfy the conditions stated previously two new gaps are created and the algorithm is iterated. The algorithm stops when no more gaps can be created.

5.1.2 Numerical results

By iterating the algorithm for multiple samples and for different aspect ratios and counting the number of segments that adsorbed, it is possible to make a statistical study of the average number of segments as a function of the aspect ratio.

From Fig. 5.2 it is possible to observe that, as predicted, the average number of particles increases with the aspect ratio. But this dependence is not trivial, especially because the curve changes when AR goes from $0 < AR < 1$ to $AR > 1$. This slight change is due to the fact that for $0 < AR < 1$ the particle can completely cover the patch. By contrast, for $AR > 1$, a single particle can never completely cover the substrate.

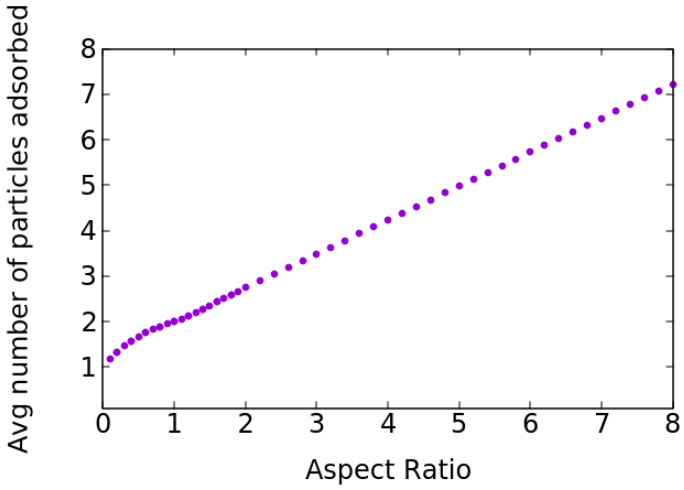

Figure 5.2: Average number of particles adsorbed as a function of the aspect ratio for the one-dimensional continuum model. The results were taken using an average over 10^6 samples.

It is also possible to calculate the average number of particles adsorbed for a very large AR, in order to compare our result to the one derived by Rényi for the *car parking problem*. Using a patch of length 10^7, and averaging over 10^5 samples, we get the result $\rho_{jam} = 0.747598(\pm 1 \times 10^{-6})$, which is consistent with the Rényi value, within error bars.

By calculating how many segments fall in the patch in each sample one can estimate the probability of falling n particles in the patch, with $n = 1, 2, 3, 4, 5$ different particles, as a function of the aspect ratio. Just like expected, for certain lengths of the patch the number of particles is limited. For example, for $0 < AR < 1$ it is only possible to fit either one or two particles.

The results were obtained averaging over 10^7 samples, and using a pseudo-random-number generator, the Marsenne Twister.

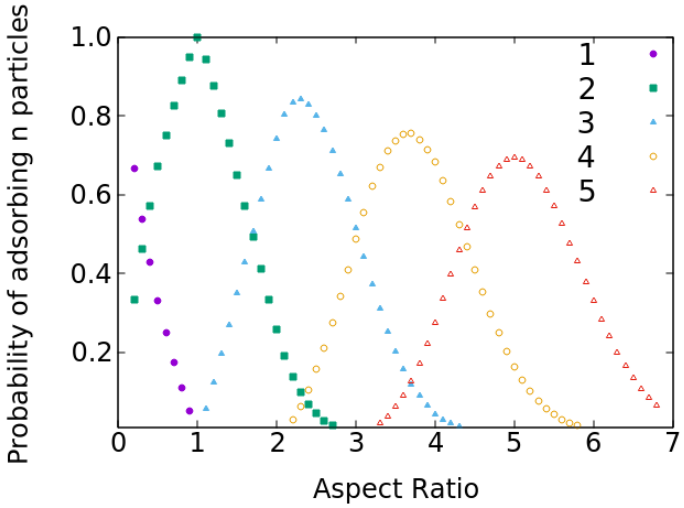

Figure 5.3: Probability of adsorbing $n = 1, 2, 3, 4, 5$ particles on the patch as a function of the aspect ratio for the one-dimensional continuum model. The results were taken using an average over 10^6 samples.

5.1.3 Analytic approach and comparison to the numerical results

We also solved this problem analytically and obtained exact expressions for a finite interval of values of AR. We use a probabilistic approach where we enumerate all possible configurations. Another reason why we treat the one-dimensional case is because it is easier to approach using this method. Increasing the dimension makes this method significantly harder to apply.

Again, we consider a substrate with size $r+1$, where the patch starts at $x = 1$ and ends at $x = r+1$. For simplicity, we consider the reference point of the particles their leftmost point, just as in the algorithm, and they also have size equal to one, so if their reference point adsorbs in the point $x = x_{ref}$, they go up to $x = x_{ref} + 1$. We calculated the quantities of interest for the cases where $0 < r < 1$ and $1 < r < 2$. For $r > 2$, the problem becomes quite complex, and approaching it using this method becomes increasingly difficult for larger patch sizes.

In the first case, where $0 < r < 1$, the problem is simple, we can only have two possible outcomes, adsorption of only one particle which means that it covers the patch completely, or adsorption of two. This is because the probability of adsorbing more than two segments equals zero ($p(n > 2) = 0$), where $p(n)$ is defined as the probability of adsorbing n particles. Therefore:

$$p(n = 1) + p(n = 2) = 1 \ . \tag{5.2}$$

So, if we obtain an expression for one of the probabilities it is trivial to obtain the other one. Below, we calculate $p(n = 2)$.

For two particles to adsorb between $1 < x < r + 1$, which is the size of the patch, a particle cannot completely cover the patch. This means that, either a particle adsorbs after the patch begins, $x = 1$, so that there is always space to the left of it, or it adsorbs before, without completely covering the patch. Thus, either the particle adsorbs on $x_{ref} > 1$ leaving space to the left where another can always adsorb, or the other case, where $x_{ref} < 1$, but since it cannot cover the entire patch there is another condition, $x_{ref} + 1 < r + 1$. Thus, by simplifying the second inequality it gives the stronger condition which is that $x_{ref} < r$. In Fig. 5.4 is a schematic of these configurations.

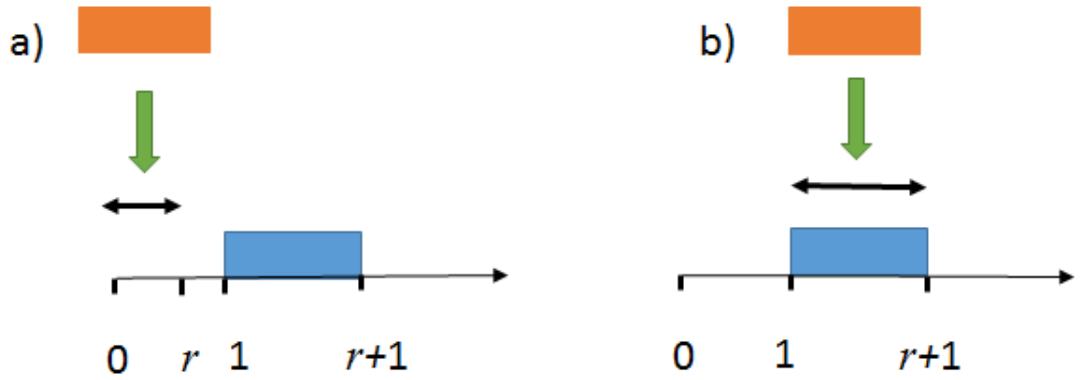

Figure 5.4: Schematic of the possible configurations when adsorbing only two particles with $0 < AR < 1$. In a), the first particle adsorbs in the interval $0 < x_{ref} < r$, while the second particle will be able to adsorb anywhere on the patch (without overlapping the first). In b), the first particle adsorbs in the interval $1 < x_{ref} < r + 1$, while the second particle will be able to adsorb anywhere on the patch.

It is important to note that a particle has equal probability of adsorbing on any point of the patch, this translates to:

$$p(x_{ref} \in [0, r+1]) = 1 \ , \tag{5.3}$$

so by normalizing one gets:

$$\int_0^{r+1} c dx_{ref} = 1 \Rightarrow c = \frac{1}{r+1} \ . \tag{5.4}$$

where c is a constant.

This means that the probability of x_{ref} being in a space between x_{ref} and $x_{ref} + dx_{ref}$ is:

$$p(x_{ref} \in [x_{ref}, x_{ref} + dx_{ref}]) = \frac{dx_{ref}}{r+1} \ . \tag{5.5}$$

Thus, making the integration in both of the considered cases where two particles can adsorb on the patch, we obtain that:

$$p(n=2) = \int_0^r \frac{dx_{ref}}{r+1} + \int_1^{r+1} \frac{dx_{ref}}{r+1} = \frac{2r}{r+1} \ . \tag{5.6}$$

Replacing back in Eq. 5.2, one gets,

$$p(n=1) = \frac{1-r}{r+1} \ . \tag{5.7}$$

Thus, in the range considered for the length of the patch, $p(n=2)$ increases with r, while $p(n=1)$ decreases. This is intuitive, because for very low aspect ratios it is more likely to be only able to fit one particle in the patch, since the particles are much larger than it. However, as soon as the aspect ratio increases and the size of the patch becomes comparable to the length of the particles, it becomes easier and more likely to have two particles adsorbed. From the two probabilities, it is possible to calculate any moment of the distribution of the number of particles per patch. For example, the first moment is

$$< n >= p(n=1) + 2p(n=2) = \frac{1+3r}{r+1} \ . \tag{5.8}$$

This analytical result agrees perfectly with the numerical result obtained using the algorithm described previously, as shown in Fig. 5.5.

It is also possible to make the same comparison for the probabilities of $p(n=1)$ and $p(n=2)$ with the numerical results, and conclude that they also are in excellent agreement (Fig. 5.6).

Let us now consider the case $1 < r < 2$. This case has some similarities with the previous one, and the first conclusion we can take is that since $r > 1$ it is impossible to only have one particle adsorbed, and therefore $p(n=1) = 0$. Also, since $r < 2$ it is also impossible to have more than three particles adsorbed, which means that $p(n > 3) = 0$. Thus, it is only possible to adsorb two or three particles in a patch with a length in the interval $1 < r < 2$:

$$p(n=2) + p(n=3) = 1 \ . \tag{5.9}$$

As before, let us first calculate $p(n=2)$. Since the maximum number of particles that can adsorb is equal to three, the reference point of the first adsorbed particle is defined as $x_{1;ref}$, while the second is $x_{2;ref}$. There are four different configurations that need to be analyzed. We define them as A,B,C and D, as described below.

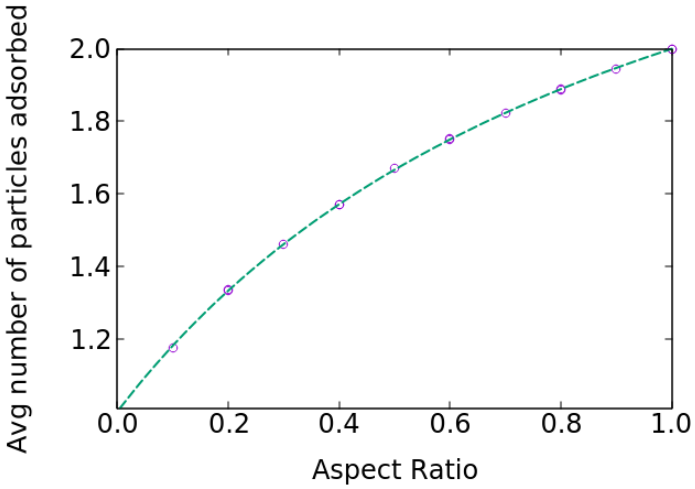

Figure 5.5: Average number of particles adsorbed on a patch with linear size in the interval $0 < r < 1$, as a function of the aspect ratio between the patch and the particle size. The purple circles represent the numerical calculations using the algorithm explained in section 5.1.1, while in a green dashed line is the analytical result, given by Eq. 5.2.

The first configuration (A) is when $x_{1;ref} \in [0, 1]$. This means that the rest of the particles can only adsorb to the right of the first one. In this configuration, to only have two particles that completely fill the patch we need to satisfy the following conditions: the first is that the distance between the endpoint of the first particle, $x = x_{1;ref} + 1$, and the reference point of the second, $x = x_{2;ref}$, is smaller than unity, which translates to the condition $x_{2;ref} - (x_{1;ref} + 1) < 1$, because in this case no other particle can adsorb between them, since they have a length of one and particles cannot overlap. The second condition is that the endpoint of the second particle, $x = x_{2;ref} + 1$, needs to surpass the endpoint of the patch, because in this case a third particle cannot adsorb to the right of the second particle (since there is no more space left in the patch), and this translates to $x_{2;ref} + 1 > r + 1$. The third condition is that the second segment cannot overlap the first, or $x_{2;ref} > x_{1;ref} + 1$.

The complication with this case is that there is a possibility of having three particles adsorbed, and we are calculating the probability of only having two. Thus, it is necessary to notice that if $r - 1 > x_{1;ref} > 1$ it is impossible to adsorb three particles, since the distance between the endpoint of the first adsorbed particle, $x_{1;ref} + 1$, and the reference point of the second, $x_{2;ref}$, will always be smaller than 1. Thus this means that if $x_{1;ref} \in [r - 1, 1]$ then $x_{2;ref} \in [x_{1;ref} + 1, r + 1]$. If on the other hand, $x_{1;ref} < r - 1$ then the possibility exists of having an empty space larger than unity between the first adsorbed particle and the second, thus, the conditions need to be more restrictive so the third particle is not able to adsorb. Considering $x_{1;ref} \in [0, r - 1]$, then $x_{2;ref} > x_{1;ref} + 1$, so they do not overlap, and $x_{2;ref} - (x_{1;ref} + 1) < 1$, so the distance between them is smaller than one and a third particle cannot adsorb. This means that $x_{2;ref} < x_{1;ref} + 2$ and $x_{2;ref} > r$ (this second condition comes from $x_{2;ref} + 1 > r + 1$, so a third does not adsorb to the right), therefore $x_{2;ref} \in [r, x_{1;ref} + 2]$. The possible configurations for this interval are represented in Fig 5.7.

In order to make the calculation of the probability for this case, it is important to remember that the probability of a particle adsorbing anywhere on the patch is equal, which for this case means that:

$$p(x_{2;ref} \in [x_{1;ref} + 1, r + 1] | x_{1;ref} \in [0, 1]) = 1 \ , \tag{5.10}$$

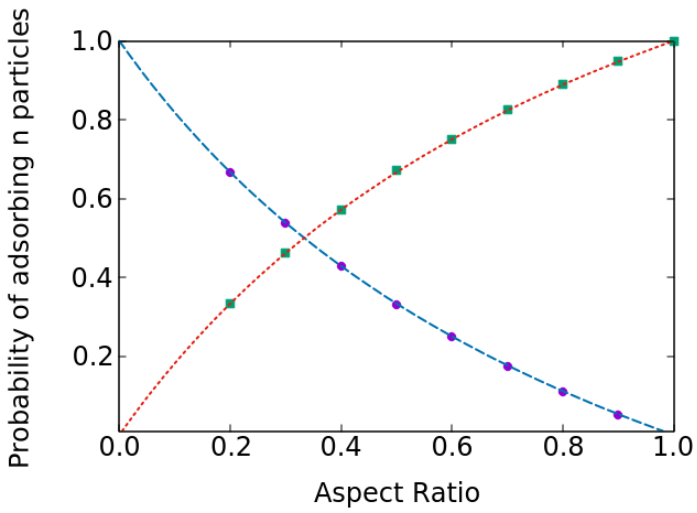

Figure 5.6: Probability of adsorbing $n = 1, 2$ particles in a patch with linear size in the interval $0 < r < 1$, as a function of the aspect ratio between the patch and the particle size. The purple circles represent the probability of adsorbing only one particle on the patch, while the green squares the probability of adsorbing two, and correspond to the numerical calculations using the algorithm explained section 5.1.1, while in a blue and orange dashed lines are the analytical results for the same probabilities, as given by Eqs. 5.7 and 5.6).

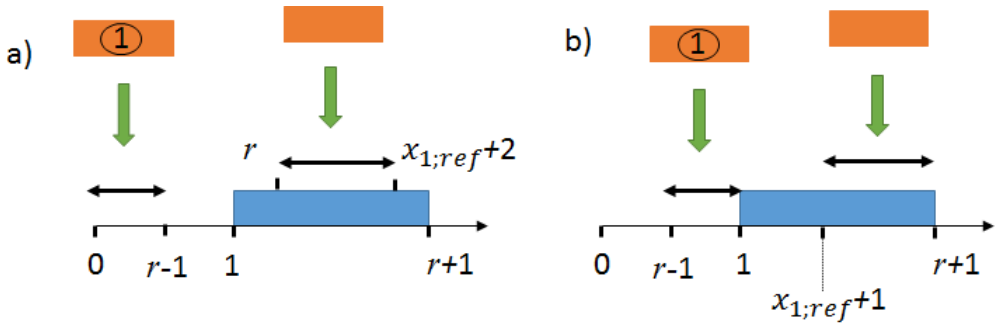

Figure 5.7: Schematic of the possible configurations when adsorbing only two particles with $1 < AR < 2$, case A. In a), the first particle adsorbs in the interval $0 < x_{1;ref} < r - 1$, while the second particle will need to adsorb in the interval $r < x_{2;ref} < x_{1;ref} + 2$, so a third cannot adsorb. In b), the first particle adsorbs in the interval $r - 1 < x_{ref} < 1$, while the second particle will need to adsorb in the interval $x_{1;ref} + 1 < x_{2;ref} < r + 1$, so a third cannot adsorb

so we can find the normalization constant, which is:

$$\int_{x_{1;ref}+1}^{r+1} c dx_{2;ref} \leftrightarrow c = \frac{1}{r - x_{1;ref}} \quad . \tag{5.11}$$

It is then possible to deduce that the probability that the second segment is in an interval between $x_{2;ref}$ and $x_{2;ref} + dx_{2;ref}$ is:

$$p(x_{2;ref} \in [x_{2;ref}, x_{2;ref} + dx_{2;ref}]) = \frac{dx_{2;ref}}{r - x_{1;ref}} \quad . \tag{5.12}$$

In conclusion the probability of $n = 2$ in this first case is:

$$p(A) = \int_0^{r-1} \frac{dx_{1;ref}}{r+1} \int_r^{x_{1;ref}+2} \frac{dx_{2;ref}}{r - x_{1;ref}} + \int_{r-1}^{1} \frac{dx_{1;ref}}{r+1} \int_{x_{1;ref}+1}^{r+1} \frac{dx_{2;ref}}{r - x_{1;ref}} \quad , \tag{5.13}$$

which gives the result:

$$p(A) = \frac{[3 - 2r + 2ln(r)]}{r+1} \quad . \tag{5.14}$$

The second case (B) is when $x_{1;ref} \in [1, r]$. In this case there will always be empty space in the patch to the left of the first adsorbed particle and to its right (since $r > 1$), and therefore $p(B) = 0$.

The third case (C) is when $x_{1;ref} \in [r, 2]$. In Fig. 5.8 is a schematic representation of this configuration. In this case, the first segment will always cover the endpoint of the patch and therefore no other particle can adsorb to the right of the first one. On the left hand side of the first adsorbed particle there is no enough space to adsorb two other ones. This means that the distance between the reference points of the first and the second adsorbed particles will always be smaller than 2. Thus:

$$p(C) = \int_r^2 \frac{dx_{1;ref}}{r+1} = \frac{2-r}{r+1} \quad . \tag{5.15}$$

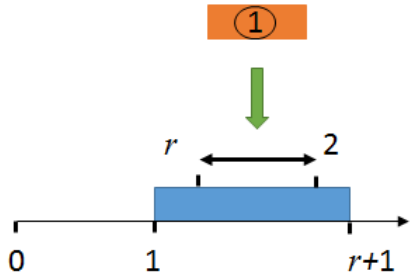

Figure 5.8: Schematic of the possible configurations when adsorbing only two particles with $1 < AR < 2$, case C. The first particle adsorbs in the interval $r < x_{1;ref} < 2$, this way the second particle will be able to adsorb anywhere on the patch (without overlapping the first), and a third will not be able to adsorb.

The fourth and last case (D) corresponds to when $x_{1;ref} \in [2, r+1]$. In Fig. 5.9 is a schematic representation of this configuration.

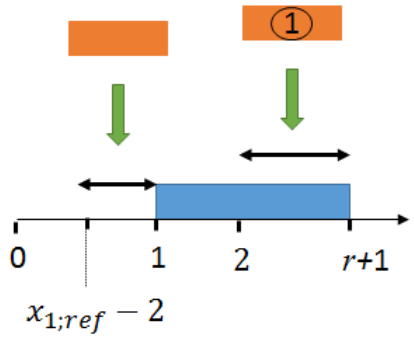

Figure 5.9: Schematic of the possible configurations when adsorbing only two particles with $1 < AR < 2$, case D. The first particle adsorbs in the interval $2 < x_{1;ref} < r + 1$, while a second adsorbs between $x_{1;ref} - 2 < x_{2;ref} < 1$. This way a third will not be able to adsorb.

In this case, after the first particle adsorbs, no other can adsorb to the right of it, and therefore $x_{2;ref} \in [0, x_{1;ref} - 1]$. But a third particle can adsorb between the first two adsorbed ones, so we need to restrict the conditions in $x_{2;ref}$. For that, it is important to note that $x_{2;ref} < 1$, otherwise

there would be enough space to adsorb another particle to the left of the second one, and also $x_{1;ref} - (x_{2;ref} + 1) < 1$. Combining both conditions, we get that $x_{2;ref} \in [x_{1;ref} - 2, 1]$, which enable us to calculate the probability of this last case:

$$p(D) = \int_2^{r+1} \frac{dx_{1;ref}}{r+1} \int_{x_{1;ref}-2}^{1} \frac{dx_{2;ref}}{x_{1;ref}-1} = \frac{2ln(r) - r + 1}{r+1} \quad . \tag{5.16}$$

Then, we can add all the these probabilities to calculate the probability of adsorbing two particles in a patch of length between $1 < r < 2$:

$$p(n=2) = P(A) + p(B) + p(C) + p(D) = \frac{2[3 - 2(r - ln(r))]}{r+1} \quad , \tag{5.17}$$

using 5.9:

$$p(n=3) = 1 - p(n=2) = \frac{5r - 4ln(r) - 5}{r+1} \quad . \tag{5.18}$$

Since we now calculated both probabilities it is possible to calculate the average number of particles:

$$< n >= 2p(n=2) + 3p(n=3) = \frac{7r - 3 - 4ln(r)}{r+1} \quad . \tag{5.19}$$

In Fig. 5.10 there is a comparison between this analytical result and the numerical one, for the average number of particles as a function of the aspect ratio, finding a very good agreement between the two. In Fig. 5.11 is a plot of the probability of having n particles adsorbed on the patch, for $1 < r < 2$. Here it is also possible to see that only $n = 2$ and $n = 3$ is different than zero, and the numerical results match very well to the analytical results derived previously.

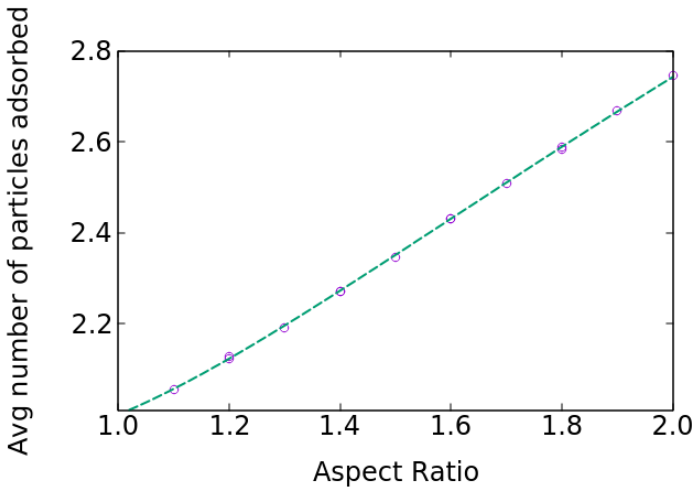

Figure 5.10: Average number of particles adsorbed on a patch with linear size in the interval $1 < r < 2$, as a function of the aspect ratio between the patch and the particle size. The purple circles represent the numerical calculations using the algorithm explained in section 5.1.1, while in a green dashed line is the analytical result, given by Eq. 5.19.

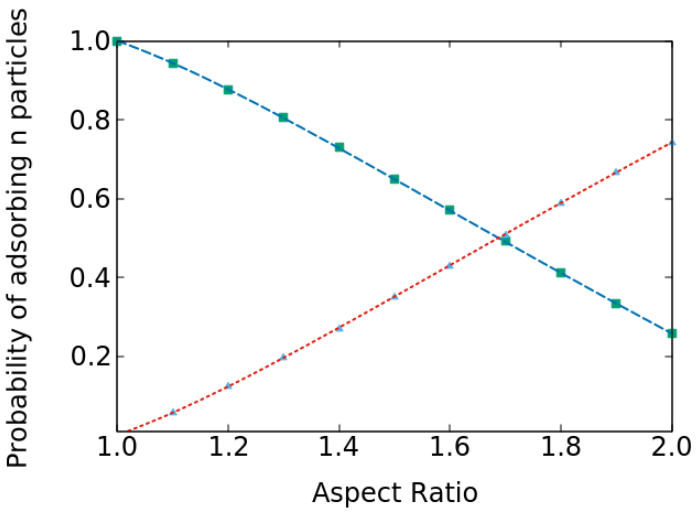

Figure 5.11: Probability of adsorbing $n = 2, 3$ particles on a patch with linear size in the interval $1 < r < 2$, as a function of the aspect ratio between the patch and the particle size. The green squares represent the probability of adsorbing two particle on the patch, while the blue triangles the probability of adsorbing two, and correspond to the numerical calculations using the algorithm explained section 5.1.1, while in a blue and orange dashed lines are the analytical results for the same probabilities, given by Eqs. 5.17 and 5.18.

Chapter 6

Conclusions

In this thesis, we studied the adsorption of DNA-coated colloidal particles on complementary functionalized oil droplets. This system is aimed at reducing the surface deformation caused by the colloidal particles when adsorbing on the oil-water interface. Using this method, it is possible to avoid long-range capillary interactions between colloidal particles that typically lead to kinetically arrested structures. Thus, it is possible to achieve a fully ergodic dynamics of colloidal particles after adsorption, where the most stable thermodynamic structures are kinetically accessible.

The physical system consists of oil droplets in a water solution which are stabilized using SDS molecules to form surfactants. To the surface of the droplets are adsorbed negatively charged PLL-PEG-bio polymer chains, which can diffuse along its surface. Then, by attaching single strands of DNA to the polymers, forming DNA patches, and covering colloidal particles with the complementary ones, it is possible to create a selective particle-substrate interaction. It is possible to show that by using this scheme the deformation of the surface is negligible, and that, although very strong, the adsorption of the colloidal particles to the surface of the droplet can be reversible by increasing the temperature. It was observed that the coverage of the oil droplet not only depends on the dynamics on its surface but also on the bulk concentration of colloidal particles.

We developed a theoretical model that grasp the most relevant physical properties of the experimental system. It consists of a substrate which is modeled as a lattice with a certain size, where patches are able to diffuse, with a certain diffusion coefficient D. Particles attempt adsorption on the substrate with flux F. Particles can only adsorb on free patches, and the particle-particle interaction, as well as the patch-patch one, is reduced to excluded volume. After a particle adsorbs on a free patch, if it still has unoccupied space bellow it, another patch that is diffusing can find it and aggregate to it. With this model it is possible to study the irreversible adsorption of the colloidal particles on mobile patches, and see how the coverage of the system depends on the dynamical parameters of the model.

One of our approaches was to use numerical simulations. To follow the time dependent dynamics a kinetic Monte Carlo method was used. Since the catalog of processes and their respective rates can be listed, it is possible to apply a rejection free algorithm for the simulations, which is very efficient to reach larger time scales when compared to others, like Brownian Dynamics. Other than that, it also makes use of a physical clock and takes into account the sequence of events leading to the the final configuration (unlike standard MC), which are important aspects when studying out-of-equilibrium systems.

We studied the model for one- and two-dimensions. In both, the patches are modeled as monomers, while the particles in one-dimension are modeled as dimers and, in two, as squares with lateral size

equal to two in units of lattice sites. We focused on the time evolution of the coverage. We observed that the coverage increases with time. For higher particle fluxes the jamming coverage of the system tends to the asymptotic value of one particle adsorbed per patch, since patches will have less time to aggregate between successive adsorptions. While for higher diffusion coefficients, it decreases, since the patch aggregation is more probable, which leads to a smaller quantity of free patches available for adsorption.

We also observed that, for earlier times, the coverage of the system has a negligible dependence on the diffusion coefficient of the patches. This is taken from the fact that the curves of the coverage as a function of time almost overlap, with the one for $D = 0$, for different diffusion coefficients. Thus, this time evolution can be divided into two regimes, the first where the system behaves as $D \approx 0$, and a second where the diffusion coefficient of the patches has an effect on the coverage. By defining a time, t^*, which measures how the curves from a certain diffusion coefficient deviate from the $D = 0$ one, it was possible to conclude that, t^* decreases with D, since the patches take less time to find previously adsorbed particles. t^* also decreases with n_0 (initial patch density), since the higher the n_0 the smaller it is the typical distance between patches, and between patches and adsorbed particles, which promotes patch aggregation. Finally, we also found that t^* decreases with F, since more particles will attempt to adsorb which will lead to a faster coverage of the system and in turn promote more patch aggregation, due to the fact that there are more particles available. These results were observed for both one- and two-dimensions.

Then we looked at how the jamming coverage depends on the parameters of the model. It was possible to observe that as the system reaches jamming, the number of relevant parameters is reduced. During the time dependent dynamics, both F and D are relevant parameters, while for the jamming state, the relevant parameter becomes the ratio F/D. We also see that the jamming coverage is a monotonically increasing function of F/D, this is due to the fact that there is a competition between two time scales, the brownian time, characteristic of the patches diffusion, and the inter-arrival time of the particles. Thus, when F/D increases more particles will be able to adsorb since patches will have less time to find adsorbed particles to aggregate between successive adsorptions. This behavior was observed in one- and two-dimensions as well. This result helps explaining the experimental observations, where they see the increase in the bulk concentration of colloidal particles (increase in F, in our model) leads to a larger coverage of the oil droplet, which is what we observe numerically.

Our next approach was to use a mean-field approximation, based on rate equations, to study the time dependence of the density of adsorbed particles and patches. By taking into account only two processes that effect the coverage of the system, particle adsorption and patch aggregation, and by neglecting space correlations, we were able to reach exact closed form equations for our initial value problem.

We were able to take the asymptotic behavior of the equations ($t \to \infty$) and see that the number of parameters that the density of adsorbed particles (which is equal to the coverage) depends on is reduced, from F and D, to the ratio F/D. For the initial behavior of the equations, by using a Taylor expansion around $t = 0$, we observed that the first two terms of the expansion of the density of adsorbed particles only depend on F and n_0, while the dependence on D only appears in the third term. Thus, while this third term is negligible, the density of adsorbed particles behaves approximately as $D = 0$. By comparing these results with the simulations data we can conclude that the functional dependencies derived analytically are also seen in a lattice model simulation, in both one- and two-dimensions.

Our last study focuses on a continuum description of the system, where we considered that the

kinetics have less relevance, and so it becomes pertinent to study what are the possible configurations of particles and patches assuming that the adsorption is irreversible. Here, we proposed a one-dimensional model where particles, which are represented as line segments with a certain size, adsorb on a patch, that is a line segment as well, with a different size. The only interactions taken into account are excluded volume ones between particles.

To study this model numerically, we developed an algorithm that focuses on open gaps on the patch where particles can adsorb without overlapping others. By tracking these gaps it is possible to formulate an efficient algorithm without rejections. We focused on the study of how the coverage of the patch depended on the ratio between the size of the particles and the patch (aspect ratio, AR). It is observed that for $AR > 1$, the number of adsorbed particles monotonically increased with the AR. For $0 < AR < 1$, since there is a probability that one particle can cover the entire patch, the dependence is different than for $AR > 1$. We were also able to calculate the jamming coverage of the system when the patch size tends to infinity, and compare it to the *car parking problem*, which we conclude is in agreement within error bars.

We developed an analytical approach to this model using a probabilistic method where we enumerate all the possible configurations. One of the challenges of this method is that, as the size of the patch increases, the number and complexity of the possible configurations also increases, so the method becomes increasingly harder to apply. We presented here the calculations for $0 < AR < 1$ and $1 < AR < 2$, and compared to the numerical results, where we conclude that both are in excellent agreement.

We finish this thesis by discussing some of the possible directions of future works. In the lattice model, the most relevant study that can be made is of the cluster growth and dynamics. If the patch size is increased to allow the formation of clusters, it would be interesting to see if any spatial or temporal pattern appears, or how the findings of this thesis are affected. It would also be interesting to develop an exact analytical approach to the model, at least for the one-dimensional case where space correlations are easier to take into account. For the continuum model, it would be interesting to try and extend the analytical scheme discussed to larger patch sizes, and possibly generalize it to any size.

Bibliography

[1] A. J. Parnell, A. L. Washington, O. O. Mykhaylyk, C. J. Hill, A. Bianco, S. L. Burg, A. J. C. Dennison, M. Snape, A. J. Cadby, A. Smith, S. Prevost, D. M. Whittaker, R. A. L. Jones, J. P. A. Fairclough, and A. R. Parker, "Spatially modulated structural colour in bird feathers," *Sci. Rep.*, vol. 5, p. 18317, 2015.

[2] J. Teyssier, S. V. Saenko, D. van der Marel, and M. C. Milinkovitch, "Photonic crystals cause active colour change in chameleons," *Nat. Comm.*, vol. 6, p. 6368, 2015.

[3] N. A. M. Araújo, C. S. Dias, and M. M. T. da Gama, "Nonequilibrium self-organization of colloidal particles on substrates: adsorption, relaxation, and annealing," *J. of Phys.: Conden. Matter*, vol. 29, p. 1, 2017.

[4] Y. Wang, Y. Wang, X. Zheng, É. Ducrot, J. S. Yodh, M. Weck, and D. J. Pine, "Crystallization of DNA-coated colloids," *Nature*, vol. 6, p. 7253, 2015.

[5] G. Doppelbauer, E. Bianchi, and G. Kahl, "Self-assembly scenarios of patchy colloidal particles in two dimensions," *J. Phys.: Conden. Matter*, vol. 22, p. 10, 2010.

[6] S. C. Glotzer and M. J. Solomon, "Anisotropy of building blocks and their assembly into complex structures," *Nat. Mat.*, vol. 6, pp. 557–562, 2007.

[7] D. Frenkel and D. J. Wales, "Colloidal self-assembly: Designed to yield," *Nat. Mat.*, vol. 10, pp. 410–411, 2011.

[8] E. Matijevic, *Fine Particles in Medicine and Pharmacy*. Berlin, Germany: Springer Science and Business Media, 2011.

[9] S. Sacanna and D. J. Pine, "Shape-anisotropic colloids: Building blocks for complex assemblies," *Curr. Op. Coll. Interf. Sci.*, vol. 16, pp. 96–105, 2011.

[10] X. Lan and Q. Wang, "DNA-programmed self-assembly of photonic nanoarchitectures," *NPG Asia Mat.*, vol. 6, p. 97, 2014.

[11] M. Lash, M. Fedorchak, J. Mccarthy, and S. Little, "Scaling up self-assembly: Bottom-up approaches to macroscopic particle organization," *Soft Matter*, vol. 11, p. 28, 2015.

[12] A. van Blaaderen, "Materials science: Colloids get complex," *Nature*, vol. 439, pp. 545–546, 2006.

[13] S.-H. Kim, S. Y. Lee, S.-M. Yang, and G.-R. Yi, "Self-assembled colloidal structures for photonics," *NPG Asia Mat.*, vol. 3, pp. 25–33, 2011.

[14] H. Ma and J. Hao, "Ordered patterns and structures via interfacial self-assembly: superlattices, honeycomb structures and coffee rings," *Chem. Soc. Rev.*, vol. 40, p. 5457–5471, 2011.

[15] G. M. Whitesides and B. Grzybowski, "Self-assembly at all scales," *Science*, vol. 295, p. 2418, 2002.

[16] A. Cadilhe, N. A. M. Araújo, and V. Privman, "Random sequential adsorption: From continuum to lattice and pre-patterned substrates," *J. of Phy.: Condens. Matter*, vol. 19, p. 6, 2007.

[17] N. A. M. Araújo, A. Cadilhe, and V. Privman, "Morphology of fine-particle monolayers deposited on nanopatterned substrates," *Phys. Rev. E*, vol. 77, p. 3, 2008.

[18] V. Garbin, "Colloidal particles: Surfactants with a difference," *Phys. today*, vol. 66, p. 68, 2013.

[19] C. S. Dias, N. A. M. Araújo, and M. M. T. da Gama, "Nonequilibrium growth of patchy-colloid networks on substrates," *Phys. Rev. E*, vol. 87, p. 3, 2013.

[20] N. A. M. Araújo, C. S. Dias, and M. M. T. da Gama, "Kinetic interfaces of patchy particles," *J. Phys.: Condens. Matter*, vol. 27, p. 19, 2015.

[21] E. Kumacheva, R. Golding, M. Allard, and E. Sargent, "Colloid crystal growth on mesoscopically patterned surfaces: Effect of confinement," *Adv. Matter*, vol. 14, pp. 221–224, 2002.

[22] C.-A. Fustin, G. Glasser, H. Spiess, and U. Jonas, "Site-selective growth of colloidal crystals with photonic properties on chemically patterned surfaces," *Adv. Matter*, vol. 15, p. 1025–1028, 2003.

[23] C. Burda, X. Chen, R. Narayanan, and M. A. El-Sayed, "Chemistry and properties of nanocrystals of different shapes," *Chem. Rev.*, vol. 105, p. 1025–1102, 2005.

[24] I. Boerasu, M. I. Vasilevskiy, M. Pereira, M. F. Costa, and M. J. M. Gomes, "Optical properties of PZT 65/35 thin films deposited by sol-gel," *Ferroelectrics*, vol. 3, pp. 187–192, 2010.

[25] J. Joo, B. Y. Chow, and J. M. Jacobson, "Nanoscale patterning on insulating substrates by critical energy electron beam lithography," *Nanno Lett.*, vol. 6, p. 2021, 2006.

[26] M. Elimelech, J. Y. Chen, and Z. A. Kuznar, "Particle deposition onto solid surfaces with micropatterned charge heterogeneity: The hydrodynamic bump effect," *Lagmuir*, vol. 19, p. 6594–6597, 2003.

[27] R. McGorty, J. Fung, D. Kaz, and V. N. Manoharan, "Colloidal self-assembly at an interface," *Mat. Today*, vol. 13, pp. 34–32, 2010.

[28] S. U. Pickering, "Emulsions," *J. of the Chem. Soc.*, vol. 91, pp. 2001–2021, 1907.

[29] E. P. Lewandowski, J. A. Bernate, A. Tseng, P. C. Searson, and K. J. Stebe, "Oriented assembly of anisotropic particles by capillary interactions," *Soft Matter*, vol. 5, pp. 886–890, 2009.

[30] B. Madivala, S. Vandebril, J. Fransaer, and J. Vermant, "Exploiting particle shape in solid stabilized emulsions," *Soft Matter*, vol. 5, pp. 1717–1727, 2009.

[31] D. Joshi, D. Bargteil, A. Caciagli, J. Burelbach, Z. Xing, A. S. Nunes, D. E. P. Pinto, N. A. M. Araújo, J. Brujic, and E. Eiser, "Kinetic control of the coverage of oil droplets by DNA-functionalised colloids," *Sci. Adv.*, vol. 2, p. 8, 2016.

[32] M. Hadorna, E. Boenzlia, K. T. Sørensena, H. Fellermanna, P. E. Hotzb, and M. M. Hanczyca, "Specific and reversible DNA-directed self-assembly of oil-in-water emulsion droplets," *Proc. Natl. Acad. Sci.*, vol. 109, p. 50, 2012.

[33] L. Parolini, B. M. Mognetti, J. Kotar, E. Eiser, P. Cicuta, and L. D. Michele, "Volume and porosity thermal regulation in lipid mesophases by coupling mobile ligands to soft membranes," *Nat. Comm.*, vol. 6, p. 5948, 2015.

[34] S. A. J. van der Meulen, G. Helms, and M. Dogterom, "Solid colloids with surface-mobile linkers," *J. of Phys.: Conden. Matter*, vol. 27, p. 23, 2015.

[35] C. A. Mirkin, R. L. Letsinger, R. C. Mucic, and J. J. Storhoff, "A DNA-based method for rationally assembling nanoparticles into macroscopic materials," *Nature*, vol. 382, pp. 607–609, 1996.

[36] A. P. Alivisatos, K. P. Johnsson, X. Peng, T. E. Wilson, C. J. Loweth, M. P. Bruchez, and P. G. Schultz, "Organization of 'nanocrystal molecules' using DNA," *Nature*, vol. 382, pp. 609–611, 1996.

[37] D. Nykypanchuk, M. M. Maye, D. van der Lelie, and O. Gang, "DNA-guided crystallization of colloidal nanoparticles," *Nature*, vol. 451, pp. 549–552, 2008.

[38] N. Geerts and E. Eiser, "DNA-functionalized colloids: Physical properties and applications," *Soft Matter*, vol. 6, pp. 4647–4660, 2010.

[39] L. Feng, L.-L. Pontani, R. Dreyfus, P. Chaikina, and J. Brujic, "Specificity, flexibility and valence of dna bonds guide emulsion architecture," *Soft Matter*, vol. 9, pp. 9816–9823, 2013.

[40] M. C. Bartelt, "Random sequential filling of a finite line," *Phys. Rev. A*, vol. 43, p. 3149, 1991.

[41] M. C. Bartelt and V. Privman, "Kinetic of irreversible monolayer and multilayer adsorption," *Int. J. Mod. Phys. B*, vol. 5, p. 2883, 1991.

[42] M. C. Bartelt and V. Privman, "Kinetics of irreversible adsorption of mixtures of pointlike and fixed-size particles: Exact results.," *Phys. Rev. A*, vol. 44, p. R2227, 1991.

[43] M. C. Bartelt and J. W. Evans, "Scaling and spatial correlations in cooperative sequential adsorption with clustering," *J. Stat. Phys.*, vol. 76, p. 867, 1994.

[44] B. Bonnier, "Random sequential adsorption of binary mixtures on a line," *Phys. Rev. E*, vol. 64, p. 066111, 2001.

[45] B. Bonnier, "On the random sequential adsorption of d-dimensional cubes," *J. Phys. A*, vol. 34, p. 10757, 2001.

[46] J. W. Evans, "Random and cooperative sequential adsorption," *Rev. Mod. Phys.*, vol. 65, p. 1281, 1993.

[47] B. Bonnier, M. Hontebeyrie, Y. Leroyer, C. Meyers, and E. Pommiers, "Adsorption of line segments on a square lattice," *Phys. Rev. E*, vol. 49, p. 305, 1994.

[48] V. Privman, "Dynamics of nonequilibrium processes: surface adsorption, reaction-diffusion kinetics, ordering and phase separation," *Trends in Stat. Phys.*, vol. 1, p. 89, 1994.

[49] N. V. Brilliantov, Y. A. Andrienko, P. L. Krapivsky, and J. Kurths, "Fractal formation and ordering in random sequential adsorption," *Phys. Rev. Lett.*, vol. 76, p. 4058, 1996.

[50] V. Privman, "Recent theoretical results for nonequilibrium deposition of submicron particles," *J. Adhesion*, vol. 74, p. 421, 2000.

[51] V. Privman (ed.), "Adhesion of submicron particles on solid surfaces," *Adhesion of submicron particles on solid surfaces, Coll. and Surfaces A*, vol. 165, Nos. 1-3, 2000.

[52] N. A. M. Araújo and A. Cadilhe, "Gap-size distribution functions of a random sequential adsorption model of segments on a line," *Phys. Rev. E*, vol. 73, pp. 051602 – 7 pages, 2006.

[53] D. C. Rapaport, *The Art of Molecular Dynamics Simulation*. Cambridge, United Kingdom: Cambridge University Press, 2004.

[54] D. Frenkel and B. Smit, *Understanding Molecular Simulation*. Massachusetts, United States of America: Academic Press, 2001.

[55] K. Binder, "Applications of Monte Carlo methods to statistical physics," *Rep. Prog. Phys.*, vol. 60, p. 487, 1997.

[56] H. C. Kang and W. H. Weinberg, "Dynamic Monte Carlo with a proper energy barrier: Surface diffusion and two-dimensional domain ordering," *J. Chem. Phys.*, vol. 90, p. 2824, 1989.

[57] K. A. Fichthorn and W. H. Weinberg, "Theoretical foundations of dynamical Monte Carlo simulations," *J. Chem. Phys.*, vol. 95, p. 1090, 1991.

[58] L. A. Ray and R. C. Baetzold, "A Monte Carlo estimation of surface diffusion by stimulating laser-induced thermal desorption," *J. Chem. Phys.*, vol. 93, p. 2871, 1990.

[59] A. B. Bortz, M. H. Kalos, and J. L. Lebowitz, "A new algorithm for Monte Carlo simulation of Ising spin systems," *J. Comp. Phys.*, vol. 17, p. 10, 1975.

[60] M. Matsumoto and T. Nishimura, "Mersenne twister: a 623-dimensionally equidistributed uniform pseudo-random number generator," *ACM Trans. on Mod. and Comp. Sim.*, vol. 8, pp. 3–30, 1998.

[61] N. Araújo, *Nonequilibrium thin-film growth: kinetics of deposition and post evolution relaxation*. Saarbrücken, Germany: Lambert Academic Publishing, 2010.

[62] P. L. Krapivsky, S. Redner, and E. Ben-Naim, *A Kinetic View of Statistical Physics*. Cambridge, United Kingdom: Cambridge university Press, 2010.

[63] V. Privman, *Nonequilibrium Statistical Mechanics in One Dimension*. Cambridge, United Kingdom: Cambridge university Press, 1997.

[64] P. J. Flory, “Intramolecular reaction between neighboring substituents of vinyl polymers,” *J. Am. Chem. Soc.*, vol. 61, p. 1518–1521, 1939.

[65] A. Rényi, “Egy egydimenziós véletlen térkitöltési problémáról,” *Publ. Math. Inst. Hung. Acad. Sci.*, vol. 3, p. 109, 1958.

Appendix A

Derivation of the mean-field equations

Here is presented an in-depth derivation of Eqs. 4.8 and 4.7. We start with the system of equations:

$$\begin{cases} \frac{d\rho_r(t)}{dt} = -\overline{F}\rho_r - \overline{D}\rho_p\rho_r \\ \\ \frac{d\rho_p(t)}{dt} = \overline{F}\rho_r \end{cases} , \tag{A.1}$$

where $\overline{F}$ and $\overline{D}$ are considered parameters that do not depend on time. Our objective is to solve these equations for the specific set of initial conditions:

$$\rho_r(t=0) = n_0 \, , \tag{A.2}$$

$$\rho_p(t=0) = 0 \, , \tag{A.3}$$

where n_0 is also a parameter that does not depend on time. Eqs. A.1 can be decoupled, obtaining:

$$\begin{cases} \ddot{\rho_r} + \overline{DF}\rho_r^2 - \frac{\dot{\rho_r}^2}{\rho_r} = 0 \\ \\ \ddot{\rho_p} + (\overline{D}\rho_p + \overline{F})\dot{\rho_p} = 0 \end{cases} . \tag{A.4}$$

These non-linear equations have exact analytic solutions for the initial conditions problem stated by Eqs. A.2 and A.3. To solve them, let us consider the second Eq. in A.4.

Making the change of variables $v(\rho_p) = \dot{\rho_p}$ and treating ρ_p as an independent variable, leads to:

$$\frac{dv(\rho_p)}{d\rho_p} v(\rho_p) + (\overline{F} + \overline{D}\rho_p)v(\rho_p) = 0 \, . \tag{A.5}$$

This way a second-order non-linear ODE is reduced to a one-order one. Factoring out $v(\rho_p)$

$$v(\rho_p)\left(\overline{F} + \overline{D}\rho_p + \frac{dv(\rho_p)}{d\rho_p}\right) = 0 \, . \tag{A.6}$$

To find the non-trivial solution, the second term is solved, which is a linear ODE, where C_1 is a constant of integration, giving,

$$v(\rho_p) = C_1 - \frac{\overline{D}\rho_p^2}{2} - \overline{F}\rho_p \, . \tag{A.7}$$

From Eq. A.7 the variables are changed back:

$$\dot{\rho_p}(t) = C_1 - \frac{\overline{D}\rho_p^2(t)}{2} - \overline{F}\rho_p(t) \, . \tag{A.8}$$

Here the initial conditions are applied to find C_1, since $\rho_p(0) = 0$ and $\dot{\rho_p}(0) = \overline{F}\rho_r(0) = \overline{F}n_0$, it is possible to get $C_1 = \overline{F}n_0$.

$$\frac{\dot{\rho_p}}{\frac{1}{2}\left(2\overline{F}n_0 - 2\overline{F}\rho_p - \overline{D}\rho_p^2\right)} = 1 \, . \tag{A.9}$$

Integrating both sides with respect to time.

$$\frac{2\tanh^{-1}\left(\frac{\overline{D}\rho_p(t)+\overline{F}}{\sqrt{\overline{F}}\sqrt{2\overline{D}n_0+\overline{F}}}\right)}{\sqrt{\overline{F}}\sqrt{2\overline{D}n_0+\overline{F}}} = t + C_2 \, , \tag{A.10}$$

which gives the final solution:

$$\rho_p = \frac{\sqrt{\overline{F}}\sqrt{2\overline{D}n_0+\overline{F}}\tanh\left[\frac{1}{2}\left(C_2\sqrt{\overline{F}}\sqrt{2\overline{D}n_0+\overline{F}} + \sqrt{\overline{F}}\sqrt{2\overline{D}n_0+\overline{F}}t\right)\right] - \overline{F}}{\overline{D}} \, . \tag{A.11}$$

Now using the initial condition Eq. A.3:

$$C_2 = \frac{2\,\mathrm{arctanh}\left(\frac{\sqrt{\overline{F}}}{\sqrt{\overline{F}+2\overline{D}n_0}}\right)}{\sqrt{\overline{F}}\sqrt{2\overline{D}n_0+\overline{F}}} \, . \tag{A.12}$$

Substituting Eq. A.12 into Eq. A.11, the solution is reached to the initial value problem:

$$\rho_p(t) = \frac{\sqrt{2\overline{FD}n_0+\overline{F}^2}\tanh\left\{\frac{1}{2}\left[2\,\mathrm{arctanh}\left(\frac{\sqrt{\overline{F}}}{\sqrt{\overline{F}+2\overline{D}n_0}}\right) + \sqrt{\overline{F}}\sqrt{2\overline{D}n_0+\overline{F}}t\right]\right\} - \overline{F}}{\overline{D}} \, . \tag{A.13}$$

The process is similar for ρ_r. Starting with the first equation in Eq. A.4 and factoring out ρ_r.

$$\ddot{\rho_r}\rho_r + \overline{DF}\rho_r^3 - \dot{\rho_r}^2 = 0 \, . \tag{A.14}$$

Then ρ_r is treated as the independent variable and the substitution $\dot{\rho_r} = v(\rho_r)$ is made, which leads to:

$$\overline{DF}\rho_r^3 - v(\rho_r)^2 + \rho_r v(\rho_r)\frac{dv(\rho_r)}{d\rho_r} = 0 \, , \tag{A.15}$$

dividing by $\rho_r/2$ one gets,

$$\frac{2v(\rho_r)^2}{\rho_r} - 2v(\rho_r)\frac{dv(\rho_r)}{d\rho_r} = -2\overline{DF}\rho_r^2 \, , \tag{A.16}$$

then by making another change of variable $p(\rho_r) = v(\rho_r)^2$ leads to $\frac{dp(\rho_r)}{d\rho_r} = 2v(\rho_r)\frac{dv(\rho_r)}{d\rho_r}$, and therefore:

$$\frac{dp(\rho_r)}{d\rho_r} - 2\frac{p(\rho_r)}{\rho_r} = -2\overline{DF}\rho_r^2 \, , \tag{A.17}$$

then multiplying by $\frac{1}{\rho_r^2}$ leads to:

$$\frac{\frac{dp(\rho_r)}{d\rho_r}}{\rho_r^2} - 2\frac{p(\rho_r)}{\rho_r^3} = -2\overline{DF}\ . \tag{A.18}$$

Making the substitution $-\frac{2}{\rho_r^3} = \frac{d}{d\rho_r}\left(\frac{1}{\rho_r^2}\right)$:

$$\frac{\frac{dp(\rho_r)}{d\rho_r}}{\rho_r^2} + \frac{d}{d\rho_r}\left(\frac{1}{\rho_r^2}\right)p(\rho_r) = -2\overline{DF}\ , \tag{A.19}$$

$$\frac{d}{d\rho_r}\left(\frac{p(\rho_r)}{\rho_r^2}\right) = -2\overline{DF}\ , \tag{A.20}$$

then integrating on both sides.

$$\frac{p(\rho_r)}{\rho_r^2} = -2\overline{DF}\rho_r + C_3\ . \tag{A.21}$$

Now changing back the variables:

$$v(\rho_r) = \pm\sqrt{-2\overline{DF}\rho_r^3 + C_3\rho_r^2}\ . \tag{A.22}$$

Since $v(\rho_r) = \dot{\rho_r}$ the minus sign in Eq. A.22 is chosen, as ρ_r is a monotonically decreasing function of time.

The value of C_3 can already be obtained from Eqs. A.2, A.3 and A.1 where it is possible to see that $\dot{\rho_r}(0) = -\overline{F}n_0$ and that $\rho_r(0) = n_0$, and after making the substitutions one can get $C_3 = \overline{F}(\overline{F} + 2\overline{D}n_0)$, which also satisfies the constrain for real solutions given by Eq. A.22, $N_0 > \rho_r(t > 0)$.

Now what is left to solve the equation:

$$\frac{\dot{\rho_r}}{\sqrt{-2\overline{DF}\rho_r^3 + \overline{F}(\overline{F} + 2\overline{D}n_0)\rho_r^2}} = -1\ , \tag{A.23}$$

As before, integrating with respect to time, one obtains:

$$\frac{2\tanh^{-1}\left[\frac{\sqrt{\overline{F}(\overline{F}+2\overline{D}n_0-2\overline{DF}\rho_r)}}{\sqrt{\overline{F}(\overline{F}+2\overline{D}n_0)}}\right]}{\sqrt{\overline{F}(\overline{F} + 2\overline{D}n_0)}} = t + C_4\ . \tag{A.24}$$

From Eq. A.24 and using Eq. A.2,

$$C_4 = \frac{2\,\mathrm{arctanh}\left[\frac{\overline{F}}{\sqrt{\overline{F}(\overline{F}+2\overline{D}n_0)}}\right]}{\sqrt{\overline{F}(\overline{F} + 2\overline{D}n_0)}}\ , \tag{A.25}$$

and therefore:

$$\rho_r(t) = \frac{\overline{F} + 2\overline{D}n_0}{\overline{D} + \overline{D}\cosh\left[\sqrt{\overline{F}(\overline{F} + 2\overline{D}n_0)}t + 2\,\mathrm{arctanh}\left(\sqrt{\frac{\overline{F}}{\overline{F}+2\overline{D}n_0}}\right)\right]}\ . \tag{A.26}$$